GEOLOGICAL SURVEY OF CANADA
OPEN FILE 1836

Morphology and Stability of Sand Ridges on Sable Island Bank, Scotian Shelf

Michael Z. Li, Edward L. King
and Carolyn Smyth

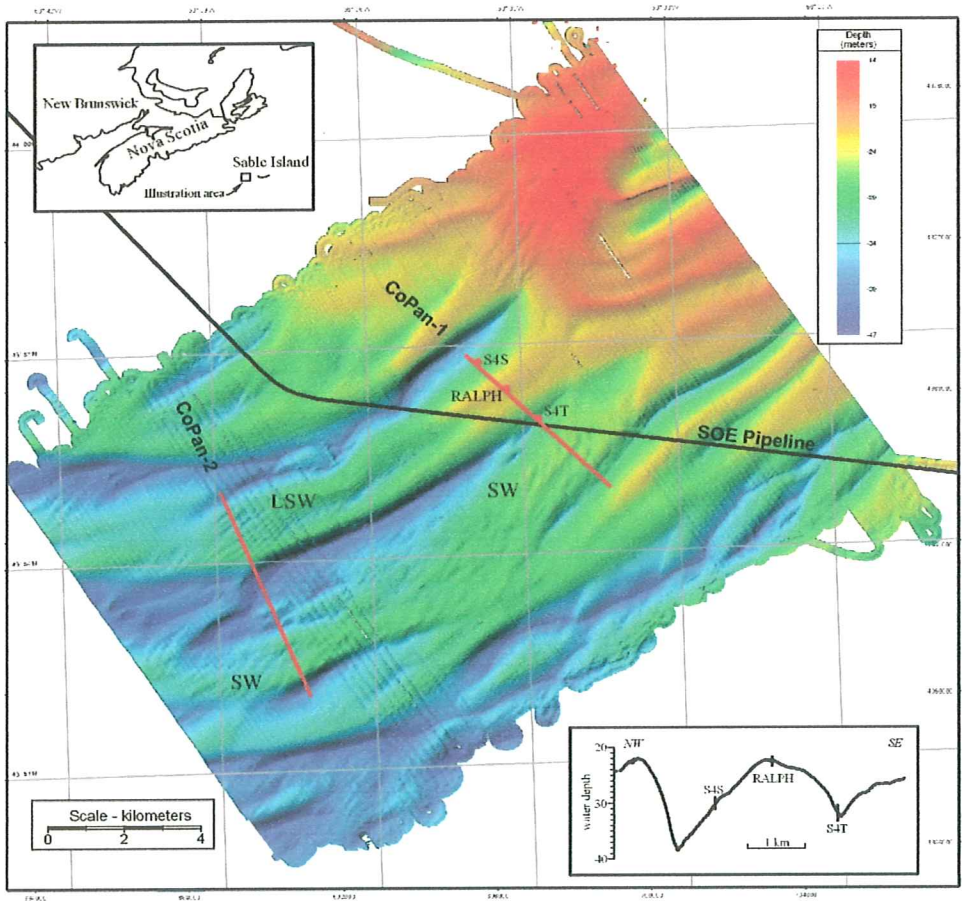

2004

Natural Resources Canada
Ressources naturelles Canada

Canada

GEOLOGICAL SURVEY OF CANADA

OPEN FILE 1836

Morphology and Stability of Sand Ridges on Sable Island Bank, Scotian Shelf

Michael Z. Li,
Edward L. King and Carolyn Smyth

2004

Available from
Geological Survey of Canada (Atlantic)
1 Challenger Drive
Dartmouth, Nova Scotia B2Y 4A2
Price subject to change without notice

Michael Z. Li, Edward L. King and Carolyn Smyth, 2004:
Morphology and Stability of Sand Ridges on Sable Island Bank, Scotian Shelf, Geological Survey of Canada, Open File 1836, 52 p.

Open files are products that have not gone through the GSC formal publication process.

TABLE OF CONTENTS

Morphology and Stability of Sand Ridges on Sable Island Bank, Scotian Shelf

Michael Z. Li, Edward L. King and Carolyn Smyth

Geological Survey of Canada (Atlantic)
Bedford Institute of Oceanography,
P.O. Box 1006, Dartmouth, N.S. B2Y 4A2

1. INTRODUCTION

Sable Island Bank, approximately 255 km long and 115 km wide, is the largest bank located on the outer Scotian Shelf (Fig. 1-1). Some of the most striking morphological features on Sable Island Bank are a series of NE-SW trending shore-face connected sand ridges. It is believed that these sand ridges were formed by aeolian and shallow marine reworking of the glacial and glacial-marine Pleistocene deposits on the bank during the last post-glacial transgression (King, 1970; Amos and Miller, 1990; King, 2001). Understanding the morphology and migration (morphodynamics) of these sand ridges will help link the hydrodynamic and sediment transport processes with the stratigraphy and the evolution of the sand body on Sable Island Bank (SIB). For offshore energy developments, the migration of these sand ridges and their superimposed bedforms can produce thick sediment mobile layers and can be hazardous to the design and safety of offshore platforms and pipelines.

Hoogendoorn and Dalrymple (1986) and Dalrymple and Hoogendoorn (1997) analyzed seismic/sidescan data and Canadian Hydrographic Service (CHS) bathymetric charts to study the morphology and internal structures of the sand ridges on Sable Island Bank. Based on ridge profiles and internal prograding bedding structures, these authors speculated that strong storm-driven flows caused the eastward migration of the sand ridges at rates as high as 50 m/year. Field measurements and model predictions of sediment transport on the Scotian Shelf (Amos and Judge, 1991; Li et al., 1997) indeed have shown that strong waves during storms work together with tidal and storm-generated currents to cause eastward net sediment transport. In contrast, Ingersoll and Ryan (1997) compared short-term repetitive multibeam surveys and 1982 CHS bathymetric charts for selected areas on SIB and found negligible to very low migration rates of the sand ridges on the bank. This conclusion, however, was not definitive because of the lower navigational resolution and density of the CHS bathymetry data.

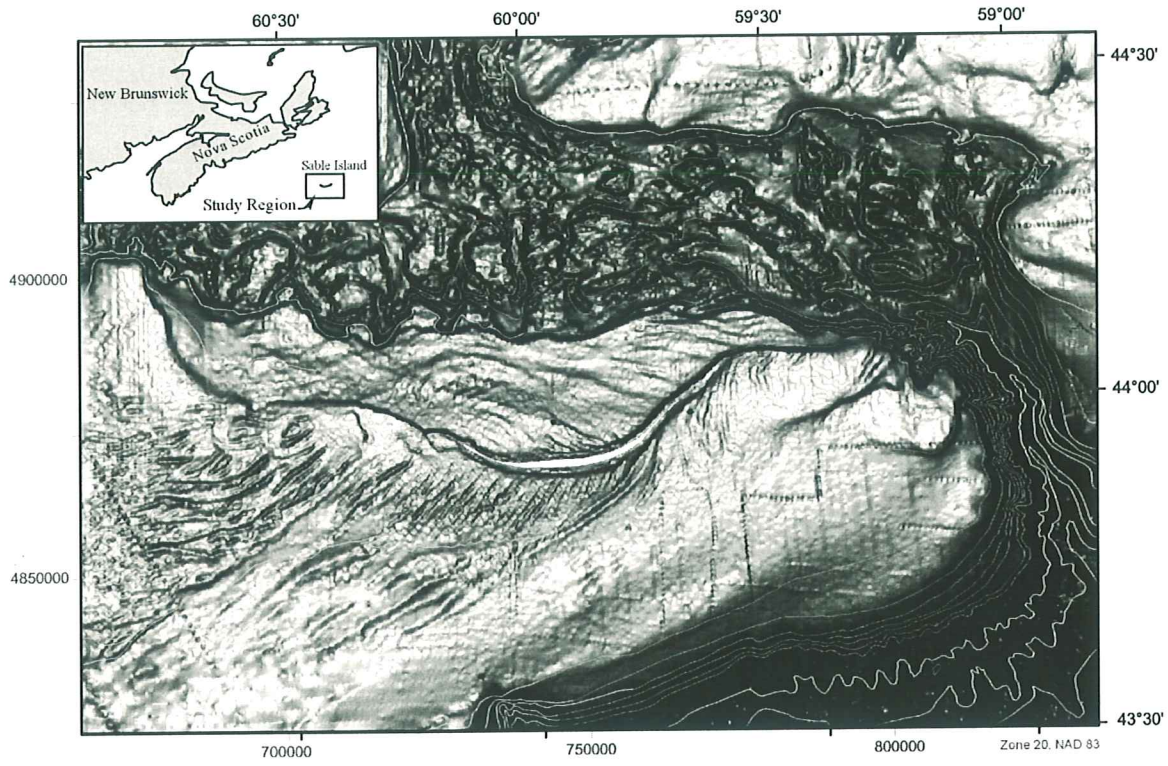

Fig. 1-1 Bathymetry map of Sable Island Bank, compiled from CHS bathymetric charts, showing the NE-SW trending shoreface-connected sand ridges.

Under the joint funding from Panel on Energy Research and Development (PERD) and Sable Offshore Energy Inc. (SOEI, now Exxon-Mobil Canada), the Geological Survey of Canada - Atlantic (GSCA) has initiated a field project to better understand the dynamics and stability of the shoreface-connected sand ridges as well as the distribution of geohazards and the regional geological framework on Sable Island Bank. Multibeam bathymetric mapping technology provides 100% bathymetric coverage of the seabed at the highest available resolution (e.g., Courtney and Fader, 1994) and its application to geological process studies has been demonstrated (e.g., Todd, et al., 1999; Courtney and Shaw, 2000). However, sidescan/seismic surveys are still required to resolve small-scale bedforms and subsurface sedimentary structures. For these reasons, repetitive multibeam bathymetry surveys have been conducted since 1996 to build up serial coverages (up to 5 years) at selected sand ridge fields on SIB in this project (Li et al., 1999; Li et al., 2001a; Li et al., 2002). Sidescan/seismic surveys as well as geological sampling and coring have also been conducted along sand-ridge transects within these sand-ridge fields (Li et al., 2001b). The results from the repetitive multibeam surveys, in combination with the sidescan survey and sampling/coring data, enable us to better define the surficial geology, morphology, and the migration rate

and direction of the sand ridges and their associated bedforms on Sable Island Bank. In addition, GSC instrumented platform RALPH and S4 wave-current meters have been deployed along sand ridge transects to simultaneously measure nearbed wave-current dynamics and sediment transport during storms at different morphological locations of a sand ridge. The processing and interpretation of these data should enable us to understand the cross-ridge variation of the hydrodynamics and sediment transport processes and how these may control the morphology and migration of the sand ridges. The objective of this report is to present and synthesize the results from the various components of the project so that a better understanding of the morphodynamics of the sand ridges on Sable Island Bank can be achieved.

2. SURVEYS AND DATA COLLECTION

2.1 Multibeam Surveys

Multibeam bathymetry data used in this report were collected from a total of 5 expeditions spanning 1996 - 2001(Fig. 2-1) on Canadian Coast Guard Ship (CCGS) Frederick G. Creed, utilizing its Simrad EM1000 system. The multibeam surveys represent an attempt to cover the sand ridges and associated bedforms at locations of different depths and hydrodynamics, and to provide serial coverage for parts of these in order to monitor temporal change and ridge migration.

Cohasset Panuke Area

The central part of the multibeam data at the Cohasset-Panuke (CoPan) site was first surveyed in 1996 on Creed96501expedition. Extensions were added to both flanks in a 1997 survey (Creed97090). On the Creed98100 expedition, the mosaic was further extended to the southwest and a repeat survey over the designated central repetitive survey area was also undertaken (Li et al., 1999). Finally, the central repetitive-survey area was surveyed for a third time on Creed 2000100 expedition with four repeat lines in the deeper southwestern area (Li et al., 2001a). Thus the essential available repetitive surveys for the CoPan area include 1996, 1998 and 2000 surveys for the central repetitive survey area.

South Sable Area

The South Sable area was initially surveyed in 1997 on the Creed97090 expedition. In 1998, the coverage

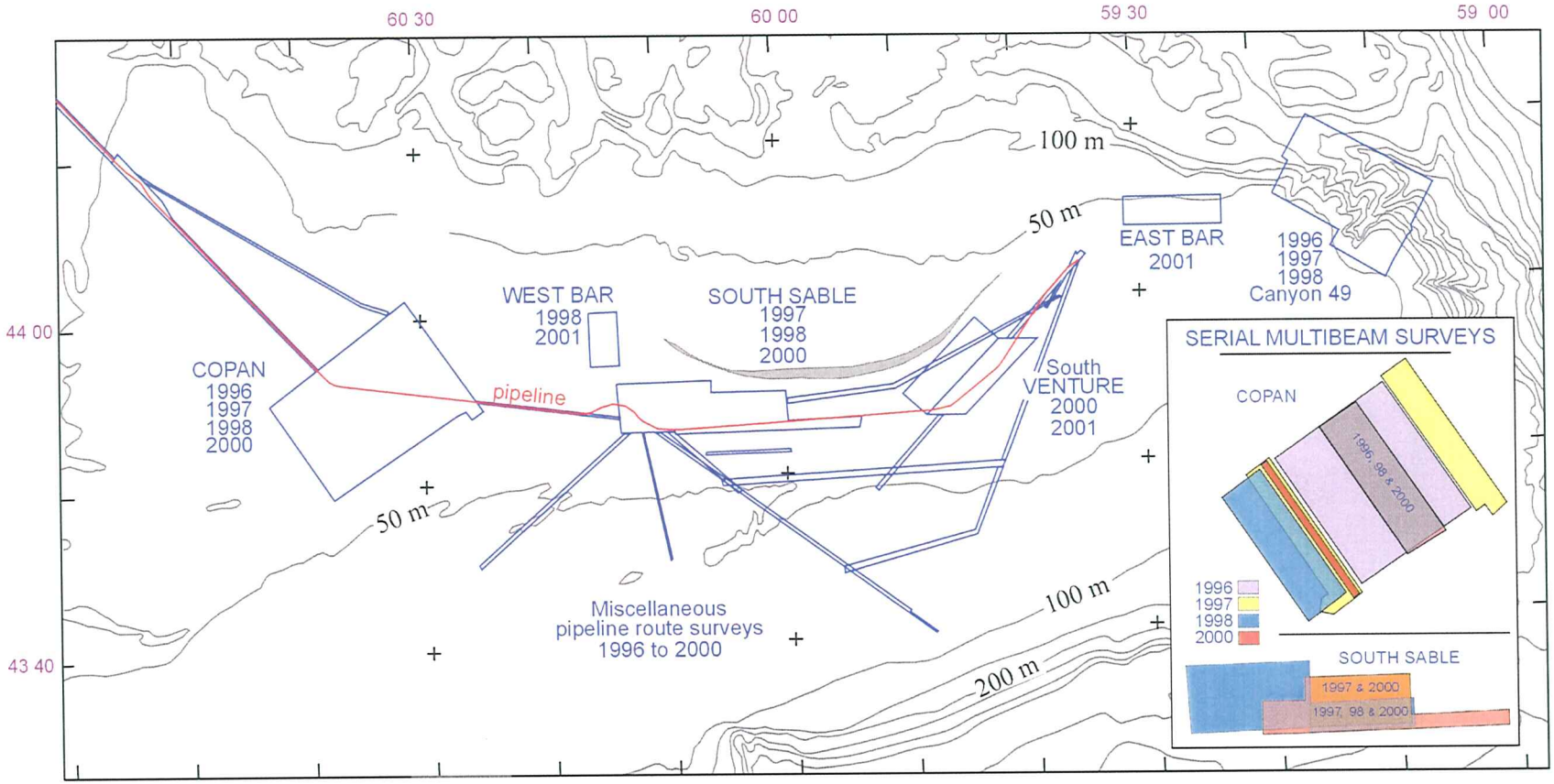

Fig. 2-1 Multibeam bathymetry surveys on SIB conducted from 1996 to 2001. Inset shows CoPan and South Sable serial coverage in detail.

was extended westward as well as a repeat survey conducted over the southern half of the 1997 survey (Li et al., 1999). In 2000, the entire 1997 survey coverage was repeated in addition to a partial eastward extension (Li et al., 2001a). The key available time series for the South Sable area thus include the overlapping 1997, 1998 and 2000 coverages over the South Sable repetitive survey area.

Multibeam surveys have also been conducted for South Venture, West Bar, and East Bar areas (Fig. 2-1), though this report focuses only on the CoPan and South Sable areas.

2.2 Hudson 2000030A Expedition

A geological/geophysical survey was conducted on CCGS Hudson in July 2000 (Li et al., 2001b). Seabed sediment samples, photographs, vibrocores and sidescan/seismic data were collected along selected sand-ridge transects at the CoPan and South Sable sites to better define the surficial geology, superposition of bedforms, and their shallow sub-surface stratigraphic structures.

2.3 In Situ Hydrodynamic and Sediment Transport Measurements

The GSCA instrumented platform RALPH (Heffler, 1996) and two InterOcean S4 current meters were deployed along a sand-ridge transect at CoPan in the winter of 2001 to obtain in situ hydrodynamic and sediment transport data over a sand ridge. This data is analyzed to help establish the relationship between hydrodynamic and sediment transport processes and sand ridge morphology and migration.

RALPH and two S4 meters were also deployed along a sand-ridge transect at South Sable in the winter of 2001/02, but the processed data and interpretation are not yet available for discussion in this report.

3. MORPHOLOGY AND SURFICIAL GEOLOGY

3.1 Sand Ridge Morphology

3.1.1 South Sable Area

The South Sable area is located to the immediate southwest of Sable Island (Fig. 2-1). The shaded-relief color bathymetry, presented in Fig. 3-1, is a mosaic compiled from surveys conducted in 1997 and 1998. Water depth is generally shallow, typically 15 - 20 m, in the northern area and gradually deepens southward to reach 30 - 40 m. There are 18 clearly defined sand ridges in the South Sable area and they are numbered as SR1 to SR18 from west to east in Fig. 3-1. Their longitudinal axes show a general NE-SW trend, though some are rotated slightly clockwise with increasing water depth, a trend common to many ridges on Sable Island Bank (Fig. 1-1).

Profiles, at 0.5 km spacing, were generated normal to the overall sand ridge orientation and were used to measure height, wavelength, symmetry and steepness (height/wavelength ratio) for various bedforms. Fig. 3-2 demonstrates the definitions of these metric parameters. The profile symmetry is defined as the ratio of the horizontal distance under the stoss (eastern) flank over that under the lee (western) flank. Table 1 lists the metrics of various bedforms measured for the South Sable area. A total of 130 measurements were obtained for sand ridges. The range of sand ridge heights is from 1.0 to 9.3 m and their average is 3.5 m. The average wavelength of sand ridges is 1.1 km with a range of 0.5 to 2.9 km. These sand ridge height and wavelength values based on multibeam data are comparable with that obtained by Hoogendoorn and Dalrymple (1986) and Dalrymple and Hoogendoorn (1997) based on hydrographic charts and seismic profiles. There is a wide range of sand ridge steepness, but the average of 0.0033 is in good agreement with previous studies (Amos and King, 1984; Hoogendoorn and Dalrymple, 1986 and Dalrymple and Hoogendoorn, 1997). The median sand ridge symmetry ranges from 0.19 to 3.24 with a median of 1.05, suggesting neutral or very slight asymmetry to the west. The histogram of sand ridge symmetry at South Sable is plotted in Fig. 3-3 which further demonstrates the mode symmetry around 1 and slightly more occurrence of sand ridges with westerly (>1) symmetry. Further examination, however, shows that there is strong local variation and that profile asymmetry can switch to opposite directions at different points along the crest lines of sand ridges. Three cross-ridge profiles (locations, Fig. 3-1) were extracted for the shallow, intermediate and deep water depths from the central part of the South Sable area. These profiles are stacked in Fig. 3-4 and demonstrate a general increase in ridge size from nearshore to offshore and a spatially variable profile symmetry. Sand ridge 8 is generally asymmetric to the west, but immediately to its east, sand ridge 9 shows overall eastward profile asymmetry. Sand ridge 10 is asymmetric to the west in the shallow and intermediate depths, but becomes symmetrical in the deep water.

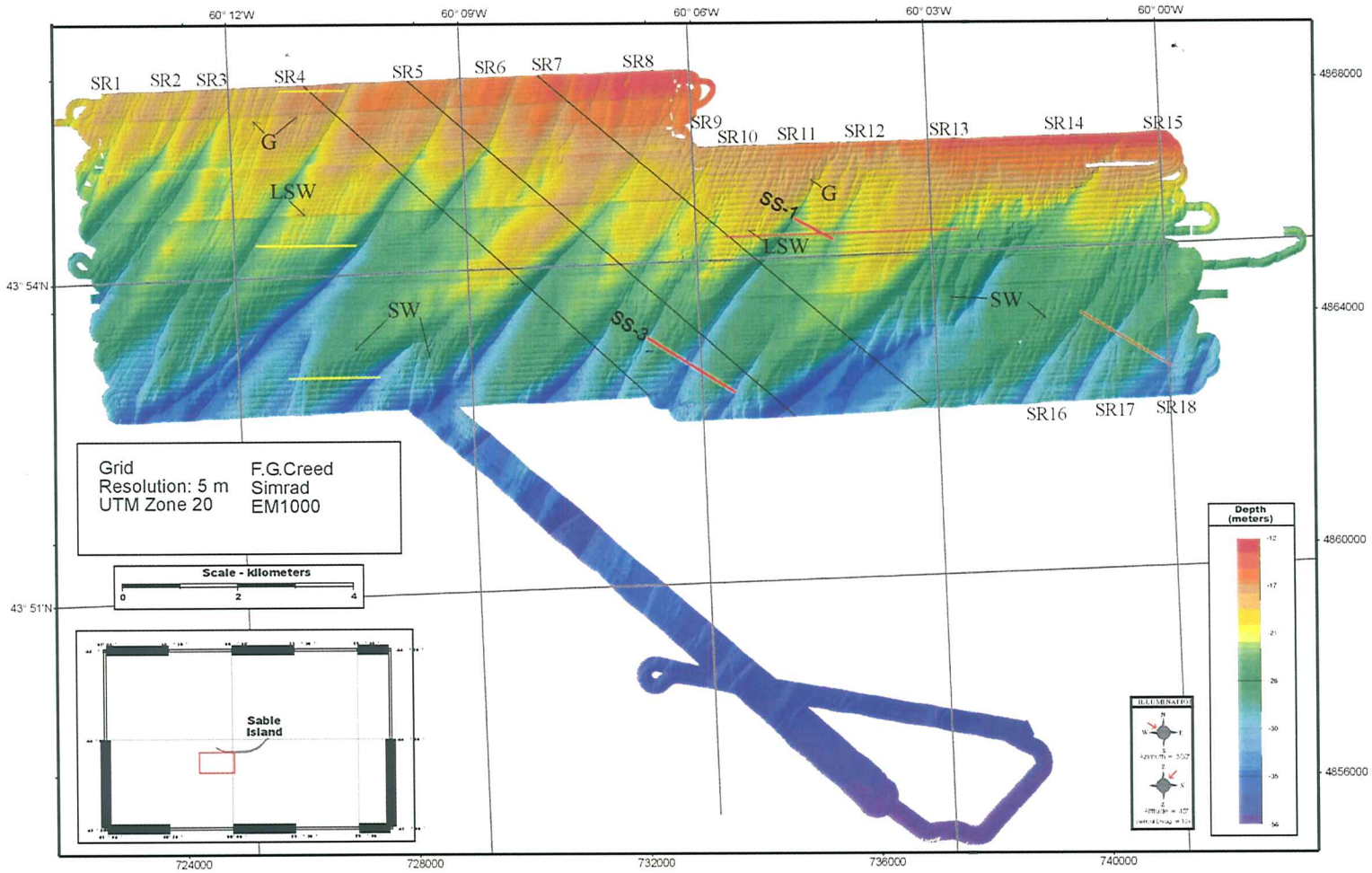

Fig. 3-1 Shaded-relief color bathymetry for South Sable showing sand ridges (marked SR1 - SR18) and superimposed sand waves (SW), linear-crest sand waves (LSW) and gutters (G). Long black lines represent the sand ridge profiles shown in Fig. 3-4. Yellow lines are the locations of SW, LSW, and gutter profiles respectively shown in Figs. 3-5 and 3-6. The thick red lines indicate the locations of sand ridge transects and the thin red lines mark the location of sand ridge profiles depicted in Fig. 4-4.

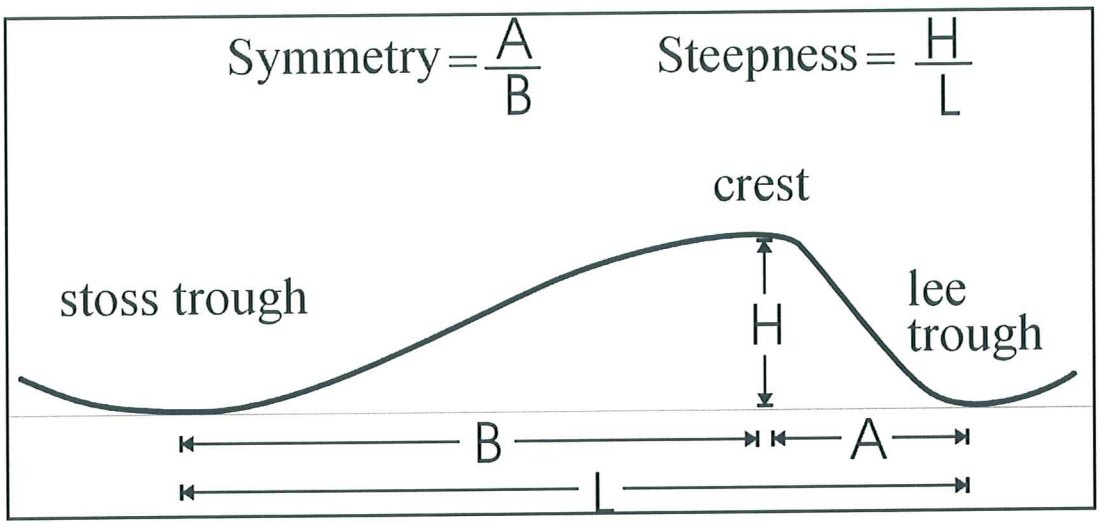

Fig. 3-2 Schematic diagram showing the definitions of various metrics parameters measured in this study: sand ridge height H, wavelength L, steepness H/L and symmetry as the ratio of the distance under the eastern flank over that under the western flank.

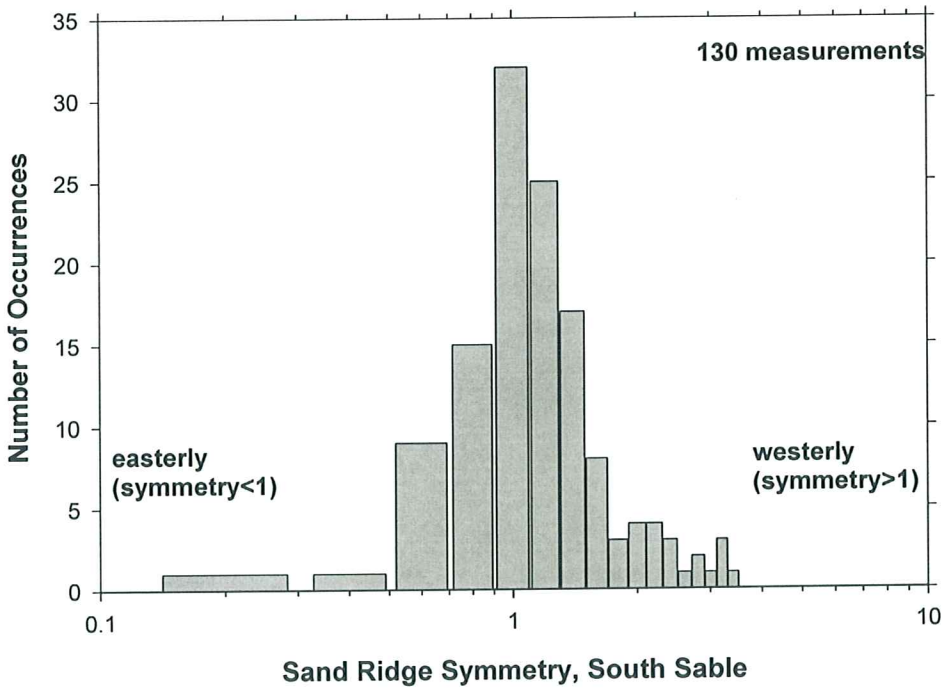

Fig. 3-3 The histogram of sand ridge symmetry for South Sable showing left-skewed distribution with a long tail of symmetry > 1.

Table 1 The metrics of various bedforms measured for the South Sable and CoPan areas respectively. Height and wavelength are in m and steepness and symmetry are dimensionless. Numbers in brackets indicate total measurements for each type of bedform.

	Minimum	Maximum	Average (median for symmetry)	Standard Deviation
Sand ridges				
South Sable area (130)				
Height	1.0	9.3	3.5	1.9
Wavelength	450	2880	1090	540
Steepness	0.0013	0.0053	0.0033	0.0012
Symmetry	0.19	3.24	1.05	0.61
CoPan area (345)				
Height	0.91	13.1	4.6	3.0
Wavelength	410	8240	1680	1330
Steepness	0.00059	0.0092	0.0031	0.0016
Symmetry	0.29	2.82	0.91	0.39
Sandwaves				
South Sable area (751)				
Height	0.09	2.88	0.45	0.33
Wavelength	21	885	130	93
Steepness	0.0009	0.0119	0.0036	0.0016
Symmetry	0.16	5.00	1.03	0.59
CoPan area (614)				
Height	0.10	4.16	0.53	0.50
Wavelength	20	990	220	150
Steepness	0.00064	0.0126	0.0029	0.0016
Symmetry	0.33	3.28	0.96	0.46
Gutters, South Sable area (141)				
Height	0.05	0.81	0.19	0.14
Wavelength	12	113	35	19
Steepness	0.0015	0.0133	0.0052	0.0022
Symmetry	N/A	N/A	N/A	N/A

Smaller bedforms can also be recognized from the multibeam mosaic in Fig. 3-1. These include low-relief degraded sand waves (SW), linear-crested sand waves (LSW), and erosional gutters (G; as defined by Myrow, 1992). Sand waves are superimposed on the flanks of sand ridges and their crests are generally oriented NNE - SSW and rotated 20^0 - 30^0 anti-clockwise from the sand ridge crest lines. In total, 751 measurements were obtained for sand waves along profiles from the South Sable area (Table 1). The heights of sand waves range from 9 cm to 2.9 m and the average is 0.45 m. The average

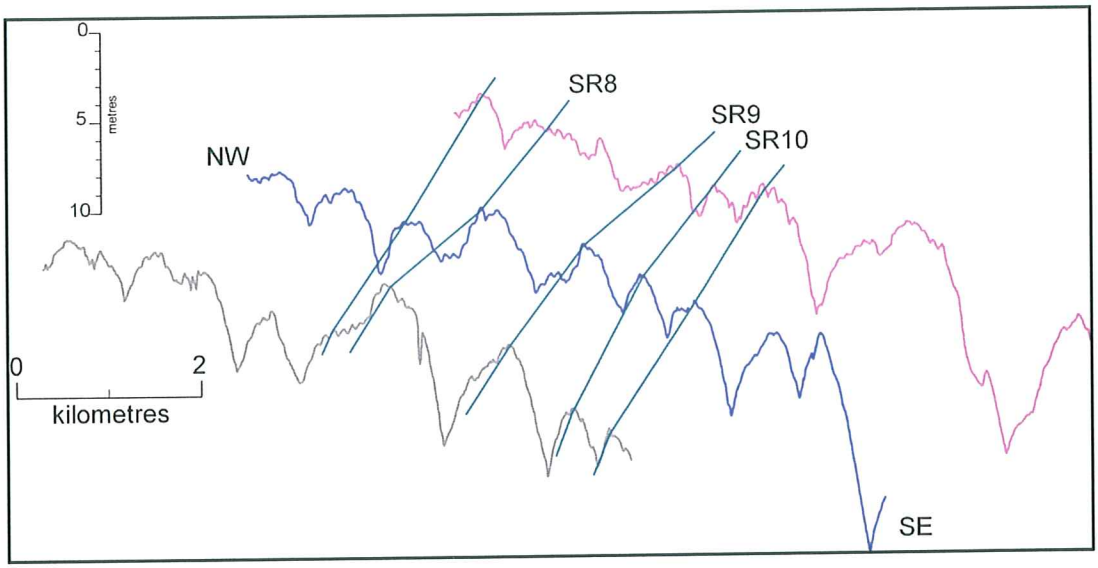

Fig. 3-4 Profiles of sand ridges from shallow to deep water from the South Sable area. The locations of these profiles are shown in Fig. 3-1. Correlations of individual ridge crests are shown with the blue lines.

wavelength is 130 m with a range of 21 to 885 m. These give an average sand wave steepness of 0.0036. This value is similar to that of sand ridges and significantly less than the established steepness of ~ 0.01 for active sand waves (Dalrymple et al., 1978; Amos and King, 1984). This reduced sand wave steepness could be due to the degradation under fair-weather conditions after their initial formation during storms. Alternatively they could have been modified by longitudinal flow erosion processes (Amos et al., 2003). The sand waves register a median symmetry of 1.03, suggesting that the profiles of sand waves at South Sable are nearly symmetrical. Based on their size and lateral continuity, sand waves can be further separated into (degraded) normal sand waves and smaller linear-crested sand waves (SW and LSW in Fig. 3-1). The average height and wavelength of the normal sand waves are 0.52 m and 154 m respectively; the values for the linear-crested sand waves are smaller, only 0.35 m and 102 m respectively. The normal sand waves are generally shorter and less coherent in orientation and spacing than the linear crested sand waves. Though they occupy similar depth range (15-35 m), the normal sand waves often occur in the intermediate to deep water while the linear-crested sand waves are mostly confined to the shallow to intermediate water depth. The profiles of normal and linear-crest sand waves (see locations in Fig. 3-1) are shown in Fig. 3-5 to demonstrate their symmetry and superimposed relationship on sand ridges. These profiles clearly demonstrate that sand waves are superimposed on both flanks of the sand ridges and that they are asymmetrical to the east on the western flanks and to the west

on the eastern flanks. This indicates that the peak mean currents through a single storm and/or during different storms could have been to either the west or the east and hence affect the sand ridge flanks differently to cause the opposite sediment transport and sand wave migration directions on the opposing sand ridge flanks. This asymmetry of sand waves, demonstrated by individual profiles in Fig. 3-5, has been confirmed at the South Sable site using overall GIS analysis. But a similar trend cannot be clearly established at the CoPan site.

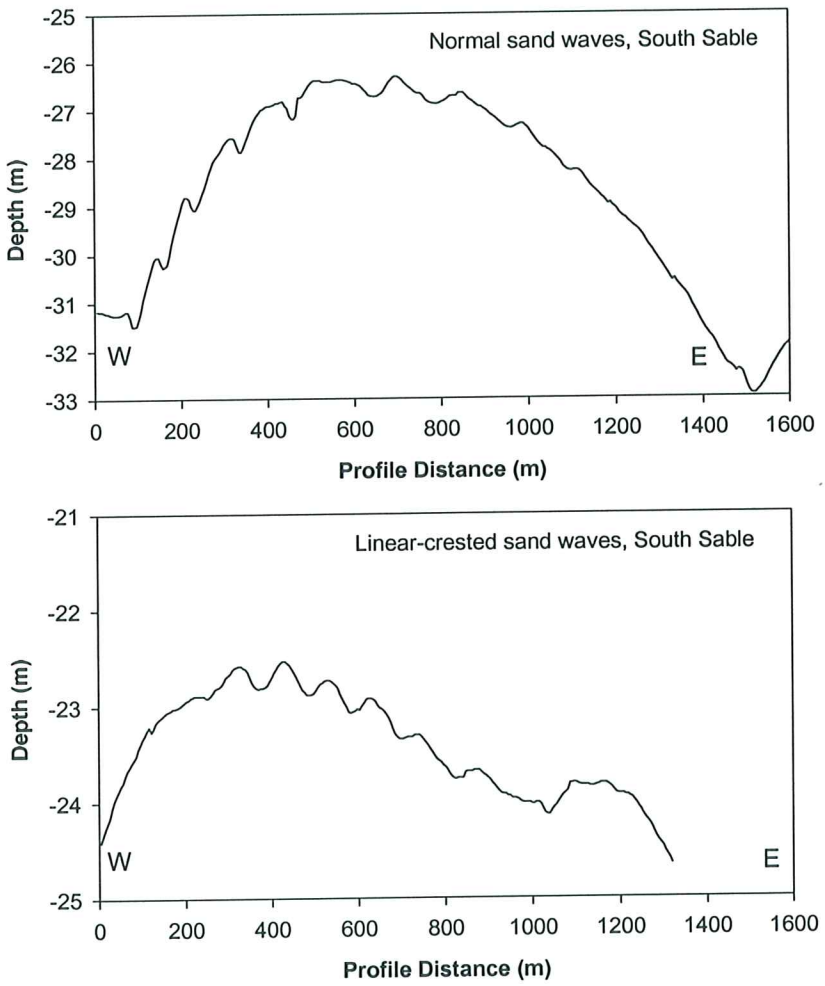

Fig. 3-5 Sand wave profiles demonstrating their symmetry and superimposing relationship on sand ridges from the South Sable area. The locations of these profiles are given by the two lower yellow lines in Fig. 3-1.

Another type of smaller bedform recognized in Fig. 3-1 is the erosional gutters (marked G in Fig. 3-1). These are shore-normal, irregularly shaped, erosional channels with low vertical relief (Myrow, 1992; Li et al., 1999; Amos et al., 2003). 141 measurements were obtained for gutters in the South Sable area (Table 1). The average spacing is about 35 m and the mean depth is only 19 cm, confirming the very low relief of these erosional features. Fig. 3-6 shows typical gutter profiles on top of a sand ridge (marked by

the upper yellow line in Fig. 3-1). The gutter channels are typically V-shaped and generally occur near the crests of sand ridges. The gutters often show steps in their channels which may indicate erosion terraces from different storms, although they are at the resolution limits of the multibeam survey system. Fig. 3-1 shows that due to the shape and steepness of channel flanks, gutters generally show sharper relief than the linear-crested sand waves lying immediately down slope from them. Gutters in the South Sable area are mostly limited to the shallow water depths (< 20 m), but some show continuation from the shallow water to intermediate depth and transform to what we have designated linear-crest sand waves. This may be an indication that some of the gutters are first formed on the shoreface by the erosion of offshore-directed undertow (down welling) during storms (Amos et al., 2003), and that as gutters extend further offshore some of them join with the offshore linear-crested sand waves. Here the "steering" or "guiding" effect of the originally formed bedforms could be a potential mechanism for the concentration of the undertow flow in the bedform troughs and hence enhance the development of gutters.

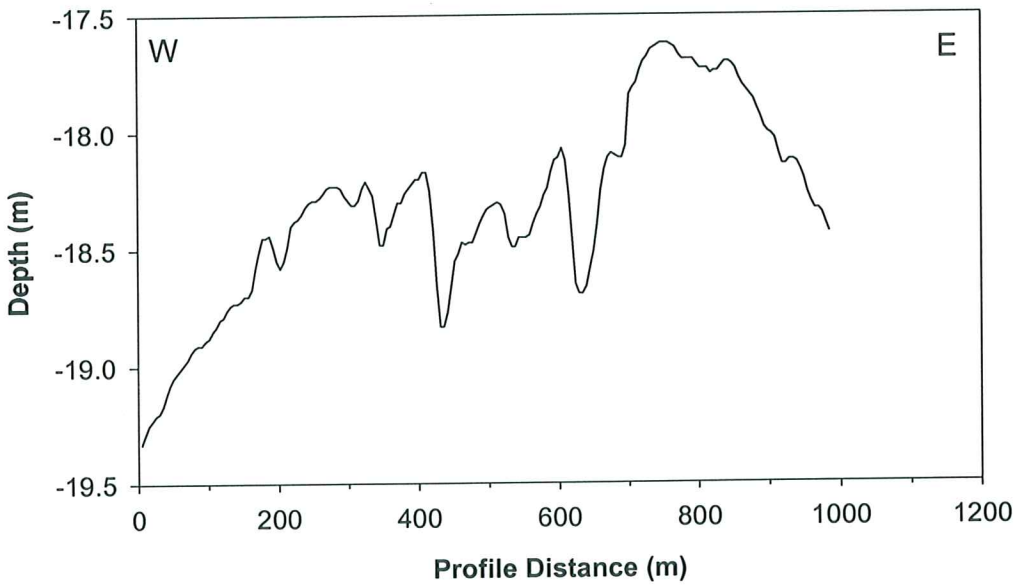

Fig. 3-6 A cross section showing typical gutter profiles on top of a sand ridge in the South Sable area. The location of the profile is marked by the upper yellow line in Fig. 3-1.

Positioning accuracy and system configurations limit the resolution of smaller bedforms (spacing < 20 m, e.g. megaripples and large wave ripples) with the EM1000 multibeam system. Sidescan data have been collected along selected sand ridge transects on Hudson2000-030A expedition (Li et al., 2001b) to register the mobility and superposition of these smaller bedforms on sand ridges. Fig. 3-7 shows the

sidescan image along the SS1 transect and extension (see Fig. 3-1 for location) which shows that sand ridge troughs are marked by dark bands due to the stronger backscatter of the gravel and coarse sand in the troughs. Low-relief 2 dimensional and linguoid megaripples, with 20-30 m wavelengths, developed in the first trough (left inset, Fig. 3-7). Large wave ripples (LWR), with about 1 m wavelength and an orientation roughly normal to the sand ridges, developed in the troughs of these megaripples. In the second sand ridge trough, however, only LWR developed on the coarse sand and gravel sediment (right inset, Fig. 3-7). Between the two troughs, the sand ridge is broadly covered by LWR (middle inset, Fig. 3-7). The color multibeam bathymetry in Fig. 3-1 shows the existence of linear-crest sand waves to the west of SS1 transect. These LSW are represented by dark linear bands in the upper-left corner in Fig. 3-7 with perpendicular LWR in the troughs of sand waves. The sidescan image along SS3 transect and extension is displayed in Fig. 3-8 and it confirms the occurrence of linear and linguoid megaripples, with LWR in their troughs, at the toe of the western flanks of sand ridges as found along SS1 transect.

3.1.2 Cohasset-Panuke Area

The Cohasset-Panuke (CoPan) area is located about 20 km to the west of Sable Island (Fig. 2-1). The mosaic of shaded-relief color bathymetry based on survey data collected from 1996, 1997 and 1998 is shown in Fig. 3-9. The shallower depths of 15-20 m in the NE corner deepen to >30 m to the SW. Eight or nine sand ridges can be recognized in this area. These sand ridges are generally NE-SW oriented in the shallower NE region but become more E-W trending in the deeper water (Fig. 3-9). Comprehensive bedform measurements along profiles similar to that for the South Sable area were also obtained for the CoPan area (Table 1). A total of 345 measurements were obtained for sand ridges in the CoPan area. In comparison with the sand ridges in the South Sable area, sand ridges in the CoPan area are generally larger: their wavelengths range from 410 m to 8.2 km with an average of 1.7 km (compared with 1.1 km at South Sable), while their heights range from 1 to 13 m with an average of 4.6 m (3.5 m at South Sable). Steepness of sand ridges at CoPan varies from 0.00059 to 0.0092 with an average around 0.0031. These are comparable with that at South Sable although the variation is wider (Table 1). The symmetry of sand ridges at CoPan ranges from 0.29 to 2.82 with a median of 0.91. In contrast to the nearly neutral overall symmetry of sand ridges at South Sable, sand ridges at Copan are moderately asymmetrical to the east. The histogram in Fig. 3-10 shows a distribution closer to normal than that of South Sable (Fig. 3-3). The size of sand ridges is found to gradually increase with water depth: the sand ridges in shallow water (depth $h < 20$ m) have a mean wavelength of 1600 m and mean height of 3.3 m . In the intermediate depth

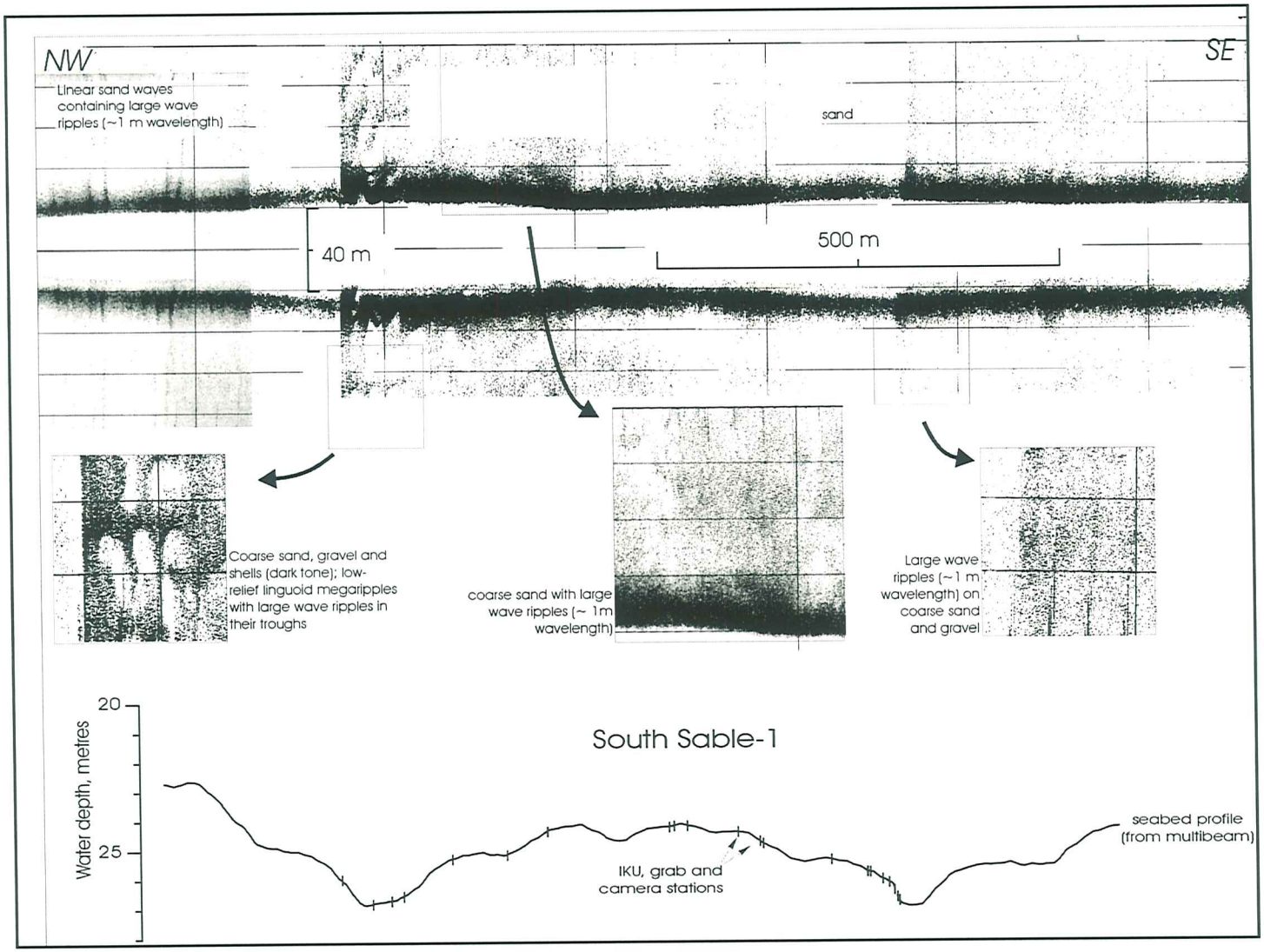

Fig. 3-7 Sidescan image collected along the SS1 transect and extension (see Fig. 3-1 for transect location).

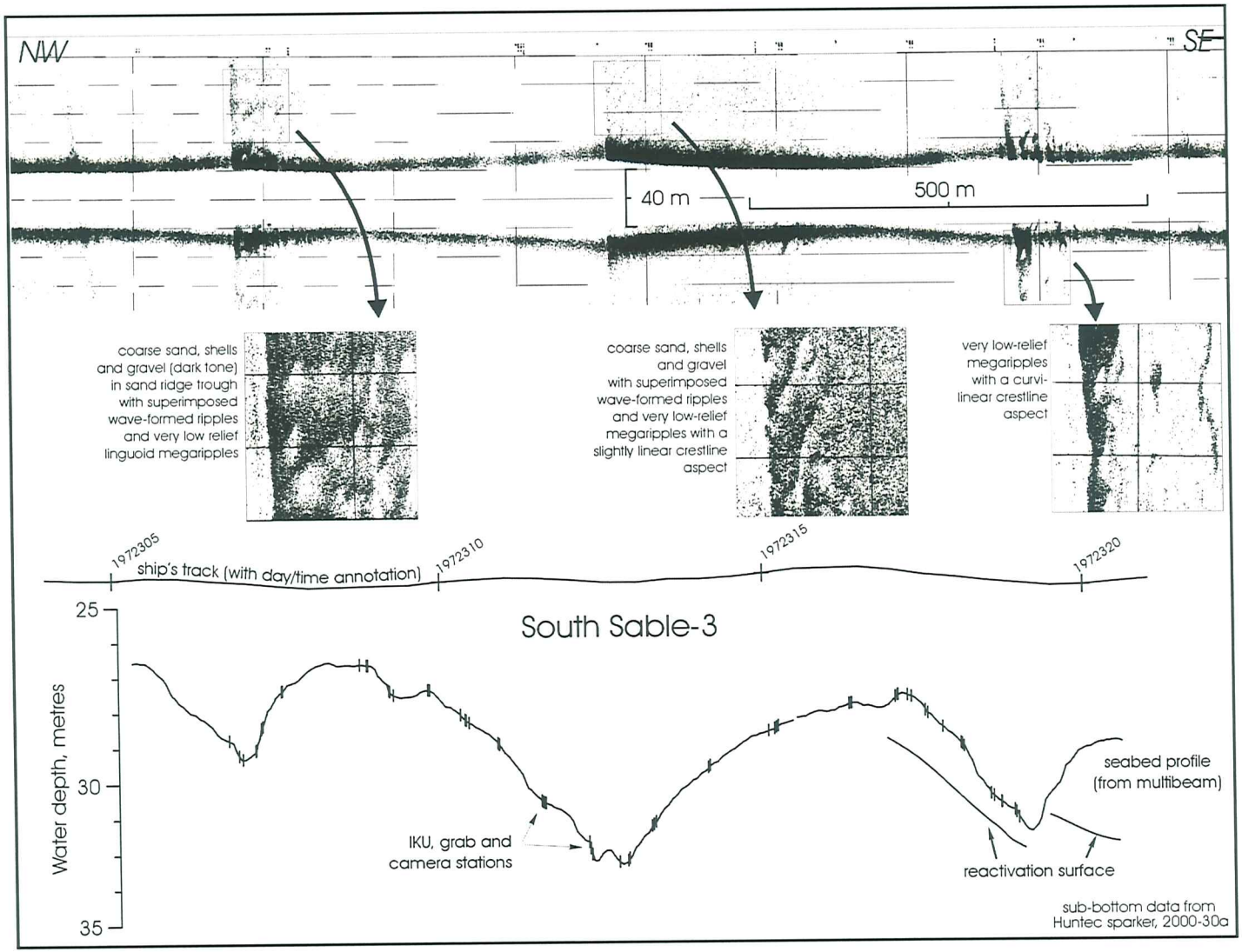

Fig. 3-8 Sidescan image collected along the SS3 transect and extension (see Fig. 3-1 for transect location).

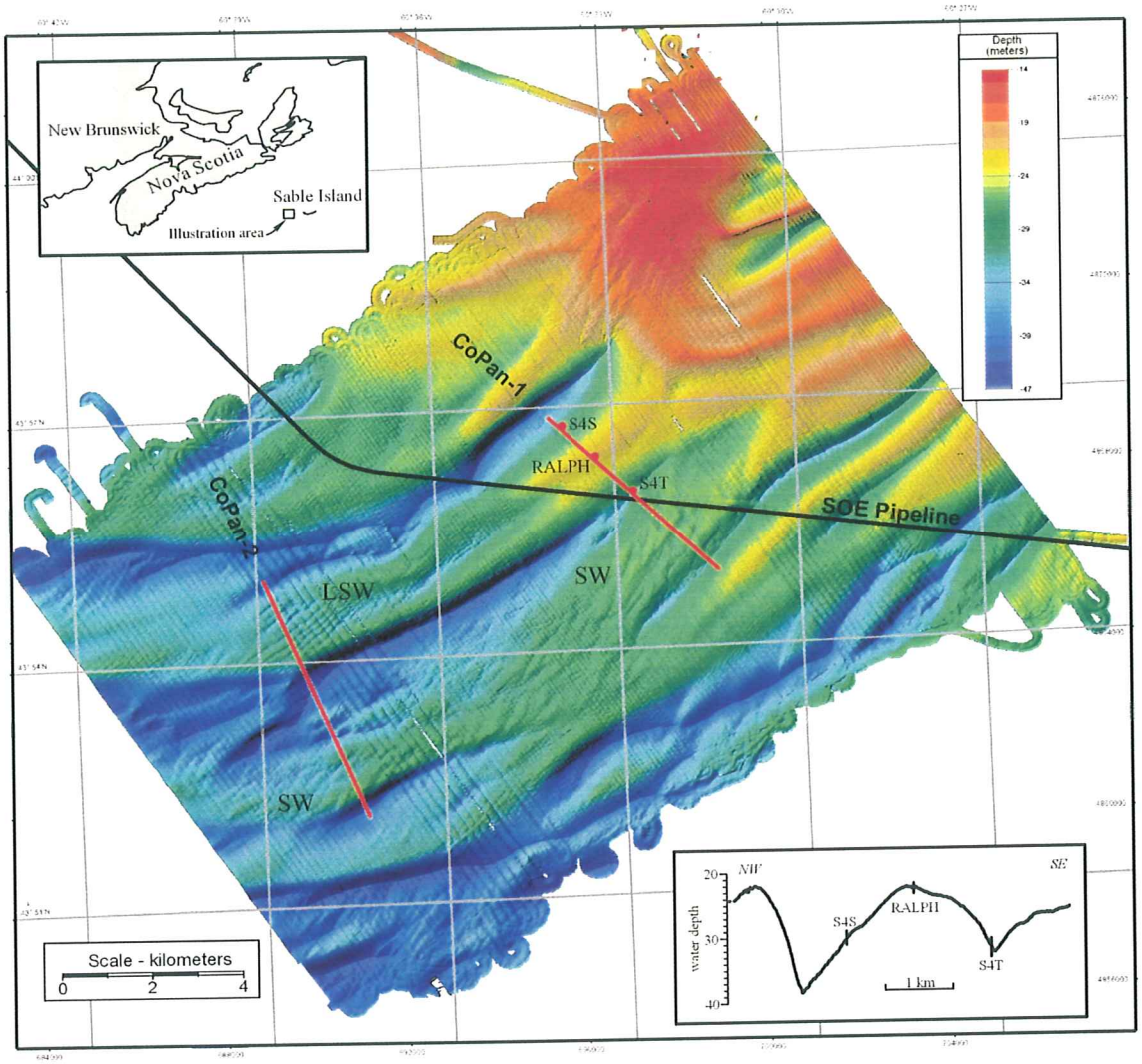

Fig. 3-9 Shaded-relief color bathymetry for CoPan based on survey data collected in 1996, 1997 and 1998 with SOEI pipeline superimposed as a heavy black line. The red lines indicate CoPan1 and CoPan2 sand ridge transects. The locations of Ralph and S4 deployments are also marked along CoPan1 transect and on the profile in the inset in the lower-right corner.

(20 m < h < 30 m), the mean wavelength and height of sand ridges increase to 1630 m and 4.7 m respectively. These values further increase to 1770 m and 5.0 m respectively in deep water (h > 30 m). In spite of great variability, sand ridges at CoPan show a general transition of profile symmetry with depth: the median symmetry is slightly asymmetrical to the west (1.04) in the shallow water, becomes nearly symmetrical (0.99) in the intermediate depth and changes to asymmetrical to the east (0.77) in the deep water.

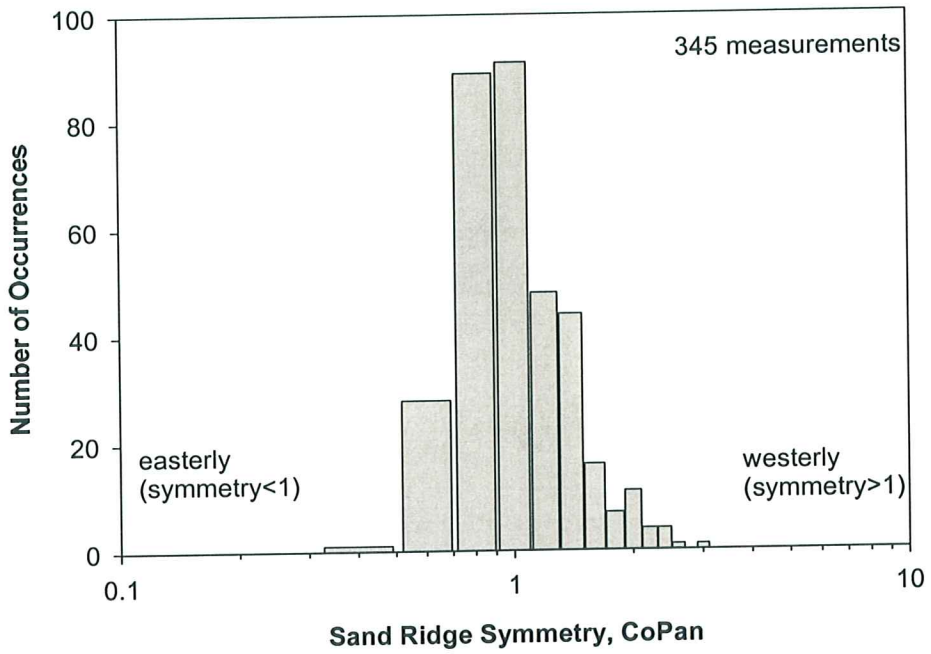

Fig. 3-10 The histogram of sand ridge symmetry for CoPan.

Degraded normal sand waves (SW) and linear-crest sand waves (LSW) are also found to be superimposed on sand ridges at the CoPan site (Fig. 3-9), although LSW are generally absent in the shallow to intermediate depths in contrast to their wide occurrences in the South Sable area. Similar to South Sable, the crestlines of the sand waves are oriented 20 - 30^0 counter clockwise relative to the ridge crests. A total of 453 metric measurements were obtained for sand waves in the CoPan area (Table 1). In comparison with the South Sable area, sand waves at CoPan are also larger. The average height and wavelength reach 0.53 m and 200 m respectively (compared with 0.45 m and 130 m respectively at South Sable). The average steepness of sand waves at CoPan is 0.0030 and is similar to that at South Sable, suggesting that sand waves at the CoPan site are significantly degraded as well. The median symmetry is at 0.96 (Table 1) and sand waves at CoPan thus show slight asymmetry to the east. Erosional gutters are not observed at the CoPan site.

A sidescan image collected along the western half of the CoPan1 transect is shown in Fig. 3-11. Linear and linguoid megaripples, with superimposed large wave ripples (LWR), are present on the eastern flank and at the toe of the western flank (left and middle insets in Fig. 3-11). The wavelengths of the

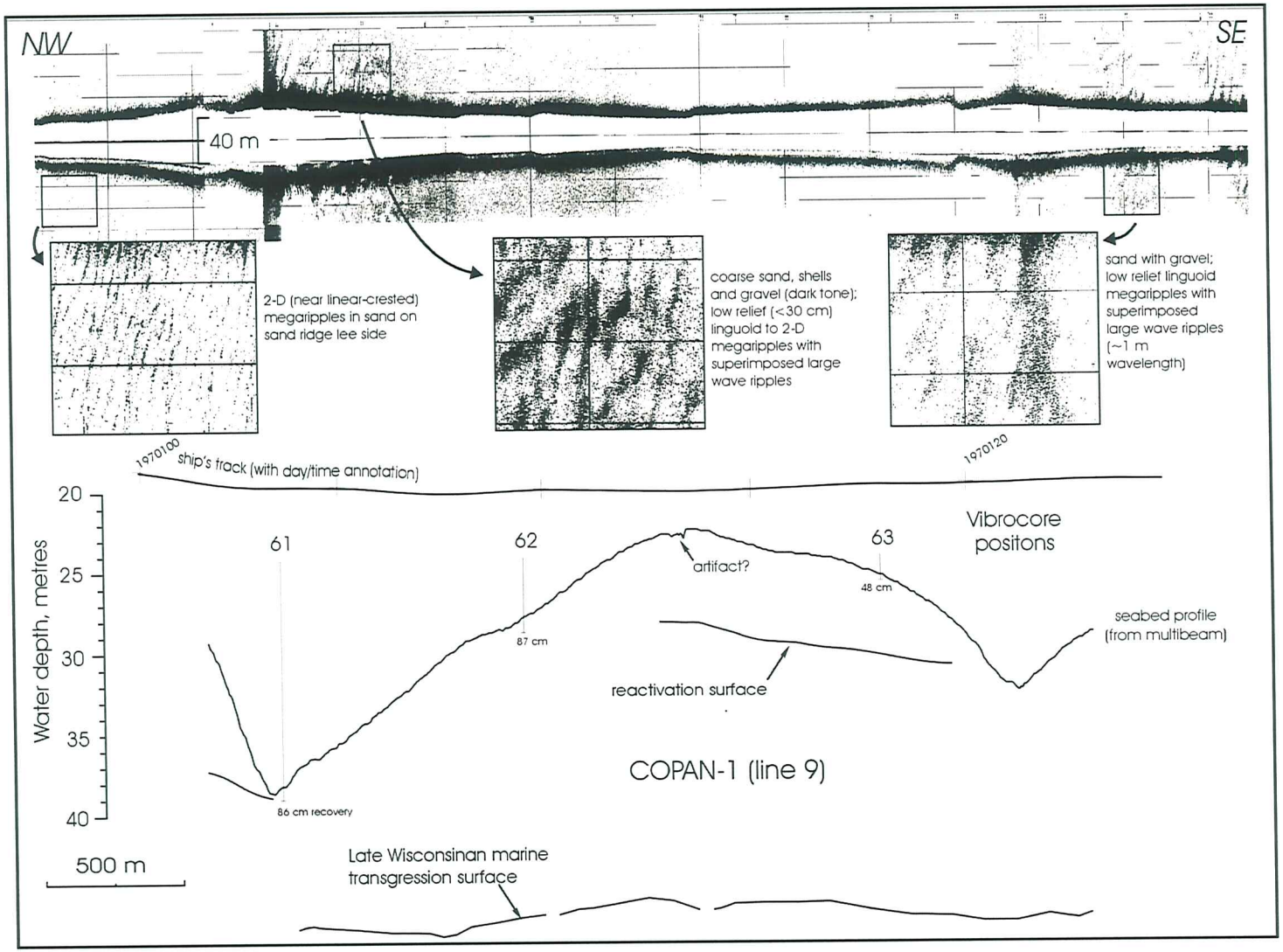

Fig. 3-11 Sidescan image collected along the western half of the CoPan1 transect (see Fig. 3-9 for transect location).

megaripples are approximately 20-30 m and their crests are oriented 20-30 degrees clockwise relative to sand ridge troughs, while LWR are generally oriented NW to SE, nearly perpendicular to the sand ridge orientation. Degraded sand waves occur as dark bands to the east of the second sand ridge trough (right area of Fig. 3-11). Linear megaripples are superimposed on the sand waves and large-wave ripples are in turn developed in the troughs of the megaripples (right inset in Fig. 3-11). The wavelength of the megaripples is approximately 30 m and again they are oriented 20-30 degrees clockwise relative to the sand waves. The wavelength of the large wave ripples is about 1-2 m and their crests trend roughly NW-SE.

3.2 Grain Size Distribution

Seabed samples were collected using a van Veen grab sampler during the July 2000 Hudson 2000030A expedition (Li et al., 2001b). These samples were analyzed for grain size parameters. Tables 2 and 3 list the grain size data and morphological locations of these grab samples along sand-ridge transects at the CoPan and South Sable sites respectively. The mean grain size (in mm) and sorting coefficient (in ϕ) along eastern halves of the CoPan 2 and South Sable 3 transects are plotted as a function of along-profile distance in Figs. 3-12 and 3-13 respectively. These figures, together with Tables 2 and 3, indicate that the seabed sediments in the trough and on the lower western flank (stoss side) are coarse or medium sand and become progressively finer from the trough toward the crest along the stoss flank to change to fine sand on the crests (Figs. 3-12 and 3-13). This trend continues eastward to the lower toe of the eastern sand-ridge flank (lee flank) before becoming coarse again in the sand ridge trough. The medium to coarse sand sediment in the trough and on the lower western flank often contain higher percentages of gravel (Tables 2 and 3), typical of winnowed erosional lag deposits. The gravel content decreases towards the crest and the eastern (lee) flank. Seabed sediment along the sand ridge transects is mostly well and very well sorted (sorting coefficients 0.3 - 0.5, Folk and Ward, 1957) except for ridge troughs and lower western flanks where sorting coefficients can be > 0.5 (moderately sorted). There is also a weak trend of across-ridge variation in sediment sorting: sediment on the sand ridge crest is best sorted and sorting becomes worse toward both troughs away from the crest.

3.3 Small Ripples on Sand Ridges

A total of 60 camera stations were conducted during the Hudson 2000030A expedition to determine the

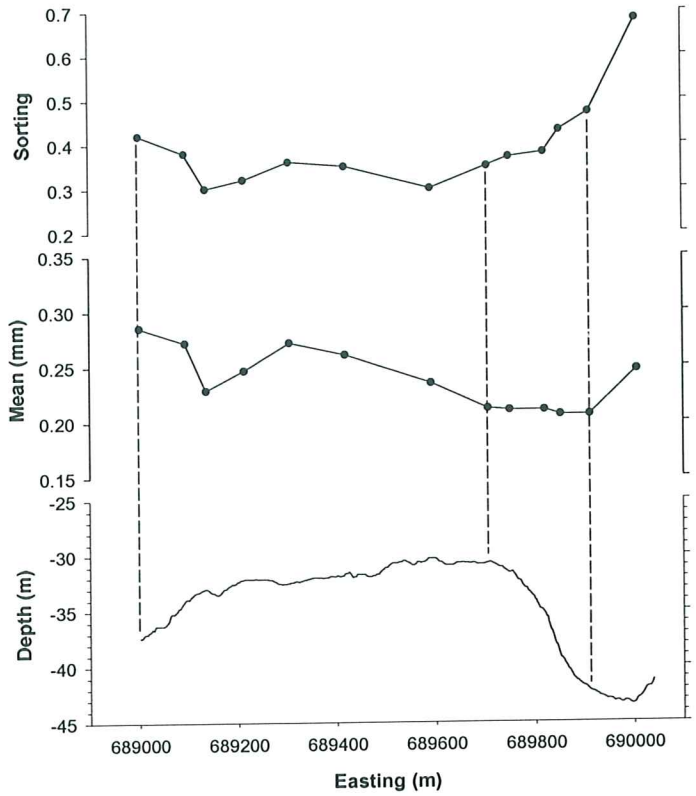

Fig. 3-12 The mean grain size (in mm) and sorting coefficient (in ϕ) along the eastern half of the CoPan2 transect.

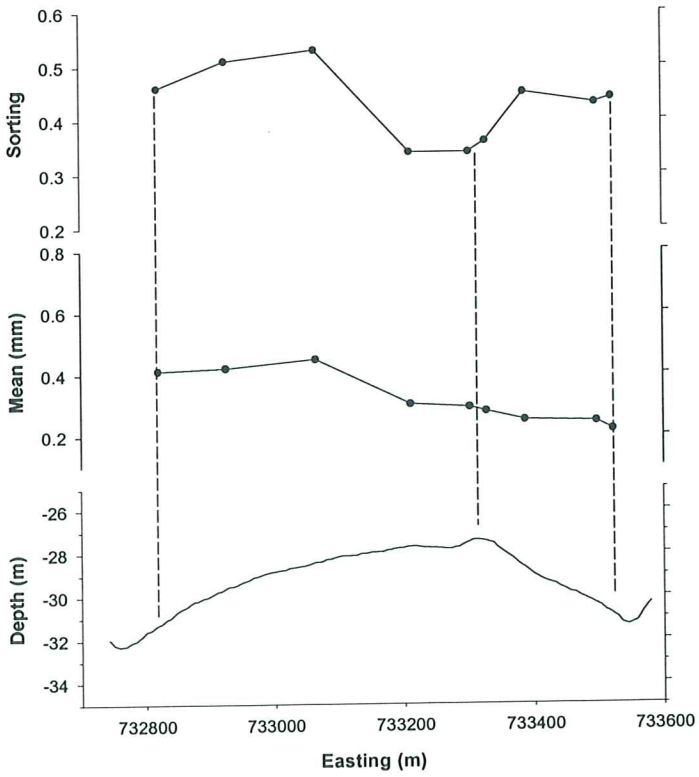

Fig. 3-13 The mean grain size (in mm) and sorting coefficient (in ϕ) along the eastern half of the South Sable 3 transect.

Table 2 List of transect station numbers, cruise station numbers, and grain size data of van Veen grab samples collected along sand-ridge transects at the CoPan site.

Transect Station#	Cruise Station#	Mean (ϕ)	Sorting (ϕ)	Gravel wt. %	Depth (m)	Location on sand ridge profile
Copan 1A						
copan-1-1	049	0.82	0.65	22.5	34	trough
copan-1-2	045	1.17	0.60	5.7	32	lower stoss flank
copan-1-3	044	1.06	0.56	7.7	30	middle stoss flank
copan-1-4	041	1.25	0.43	0.9	29	middle stoss flank
copan-1-5	040	1.07	0.43	3.3	24	upper stoss flank
copan-1-6	037	1.39	0.36	0.8	23	crest
copan-1-7	036	1.45	0.32	0.2	25	upper lee flank
copan-1-8	031	1.55	0.35	0.1	27	middle lee flank
copan-1-9	030	1.74	0.35	0.4	30	lower-middle lee flank
copan-1-10	026	1.89	0.35	0.1	32	lower lee flank
Copan 1B						
copan-1-12	021	1.46	0.41	0.3	34	lower stoss flank (or trough)
copan-1-13	020	1.55	0.40	0.3	29	lower stoss flank
copan-1-14	016	1.55	0.40	0.4	27	middle stoss flank
copan-1-15	015	1.49	0.40	0.4	25	upper-middle stoss flank
copan-1-16	012	1.44	0.39	0.5	26	crest
copan-1-17	010	1.23	0.42	1.7	29	upper lee flank
copan-1-18	006	1.33	0.45	1.7	29	middle lee flank
copan-1-19	005	1.34	0.40	0.3	31	lower-middle lee flank
copan-1-20	001	1.56	0.43	0.4	34	lower lee flank (or trough)
Copan 2						
copan-2-3	055	1.81	0.42	0.1	39	trough
copan-2-4	056	1.88	0.38	0.1	35	lower stoss flank
copan-2-6	060	2.13	0.30	0	34	lower middle stoss flank
copan-2-7	064	2.02	0.32	0	32	middle stoss flank
copan-2-8	068	1.88	0.36	0.1	33	middle stoss flank
copan-2-9	069	1.94	0.35	0	32	upper-middle stoss flank
copan-2-11	073	2.09	0.30	0.1	32	crest
copan-2-13	074	2.24	0.35	0.1	33	upper lee flank
copan-2-14	077	2.25	0.37	0	33	upper-middle lee flank
copan-2-15	079	2.25	0.38	0.1	37	middle lee flank
copan-2-16	082	2.28	0.43	0	41	lower-middle lee flank
copan-2-17	084	2.28	0.47	0	44	lower lee flank
copan-2-18	087	2.02	0.68	0.5	44	trough

Table 3 List of transect station numbers, cruise station numbers, and grain size data of van Veen grab samples collected along sand-ridge profiles at the South Sable site.

Transect Station#	Cruise Station#	Mean (ϕ)	Sorting (ϕ)	Gravel wt%	Depth (m)	Location on sand ridge profile
South Sable 1						
ss-1-2	149	1.14	0.64	5.1	24	lower western flank
ss-1-3	150	1.42	0.62	2.1	24	lower western flank
ss-1-4	151	1.06	0.50	3.7	23	middle western flank
ss-1-5	152	1.10	0.45	1.8	22	upper-middle western flank
ss-1-6	153	1.18	0.49	3.4	22	upper western flank
ss-1-7	154	1.46	0.45	0.4	22	crest
ss-1-8	155	1.26	0.43	0.8	22	upper eastern flank
ss-1-9	156	1.10	0.48	2.7	22	upper-middle eastern flank
ss-1-10	157	1.56	0.41	0.1	25	middle eastern flank
ss-1-11	158	1.74	0.43	0.1	26	lower-middle eastern flank
ss-1-12	159	1.80	0.45	0.1	26	lower eastern flank
ss-1-13	142	1.44	0.57	1.7	26	trough
South Sable 3A						
ss-3-1	089	1.30	0.58	5.7	29	trough
ss-3-2	092	1.45	0.42	0.4	29	lower-middle lee flank
ss-3-3	094	1.50	0.42	0.2	28	upper-middle lee flank
ss-3-4	101	2.11	0.40	0.1	27	crest
ss-3-5	103	2.20	0.39	0.1	28	upper stoss flank
ss-3-6	106	2.24	0.41	0.1	28	upper-middle stoss flank
ss-3-7	107	2.22	0.41	0	29	upper-middle stoss flank
ss-3-8	111	2.24	0.37	0	30	middle stoss flank
ss-3-9	112	2.34	0.38	0.1	31	lower-middle stoss flank
ss-3-10	116	2.30	0.42	0.1	32	lower stoss flank (or trough)
South Sable 3B						
ss-3-12	120	1.28	0.46	1.7	33	lower stoss flank
ss-3-13	132	1.25	0.51	2.3	32	middle stoss flank
ss-3-14	130	1.16	0.53	6.2	30	middle stoss flank
ss-3-15	127	1.73	0.34	0.1	29	upper stoss flank
ss-3-16	125	1.78	0.34	0.1	29	crest
ss-3-17	122	1.85	0.36	0.1	29	crest or upper lee flank
ss-3-18	135	2.01	0.45	0.4	30	upper-middle lee flank
ss-3-19	137	2.04	0.43	0.1	31	lower-middle lee flank
ss-3-20	141	2.21	0.44	0.6	31	lower lee flank

variation of small-scale bedforms along sand-ridge transects in summer fairweather conditions. Details of this variation have been described in Li et al. (2001b). At CoPan, seabed photos collected along the CoPan2 transect (Fig. 3-14) demonstrate ripple distribution across sand ridges. Under fairweather

conditions, the sand ridge troughs are characterized by a brownish, bioturbated bed covered by a thin layer of organic-rich fine sand (photo A in Fig. 3-14). At the lower stoss or lower lee flanks, the thin layer of fine sand develops into small current or wave ripples on top of larger inactive bedforms (photos B and C of Fig. 3-14). At both the mid-stoss and mid-lee flanks, sinuous current ripples become dominant (D and E of Fig. 3-14). Effects of waves and tidal currents become stronger at the upper flanks and on the crests of sand ridges, sinuous current ripples have further developed into three-dimensional linguoid current ripples (photo F of Fig. 3-14).

In the South Sable area, small ripples on sand ridges show similar along-transect variation. However, small wave ripples dominate at South Sable as opposed to current ripples at CoPan apparently due to the shallower water depth at the South Sable site (see details in Li et al., 2001b).

3.4 Shallow Sedimentary Structures

IKU grab samples, vibrocores, and seismic data were also obtained on the Hudson 2000030A expedition. Resin peels have been obtained from box cores pushed into the IKU grab samples. These resin peels are generally 30 by 40 cm in size and are used to demonstrate the variation of shallow sedimentary structure along sand ridge transects. Geological sections and vibrocores have been analyzed to derive updated stratigraphy and geological evolution of the sand ridges on SIB. These are the focus of a technical report submitted to Sable Offshore Energy Inc. (King, 2002).

A total of 59 resin peels were obtained from 30 IKU stations. As described in detail in Li et al. (2001b), the top 30-50 cm of the sand ridge surficial sediment shows typical storm event bed structure: The lower portion of the peels is characterized by cross lamination or bedding of medium to high angles. This is then cut and overlain by hummocky cross stratification (HCS) and/or swaley bedding in the middle section, which is in turn overlain by ripple cross stratification and parallel or low-angle cross beddings at the top of the peels. Following Swift et al. (1986) and Amos et al. (1996), the medium to high-angle cross lamination/bedding is formed by the development and migration of megaripples during the peak and early decay of a storm. HCS and swaley bedding correspond with the formation of hummocky or low-relief megaripples at the waning stage of the storm, while ripple cross stratification and parallel or low-angle cross beddings at the top of the event bed result from the development of ripples at the termination

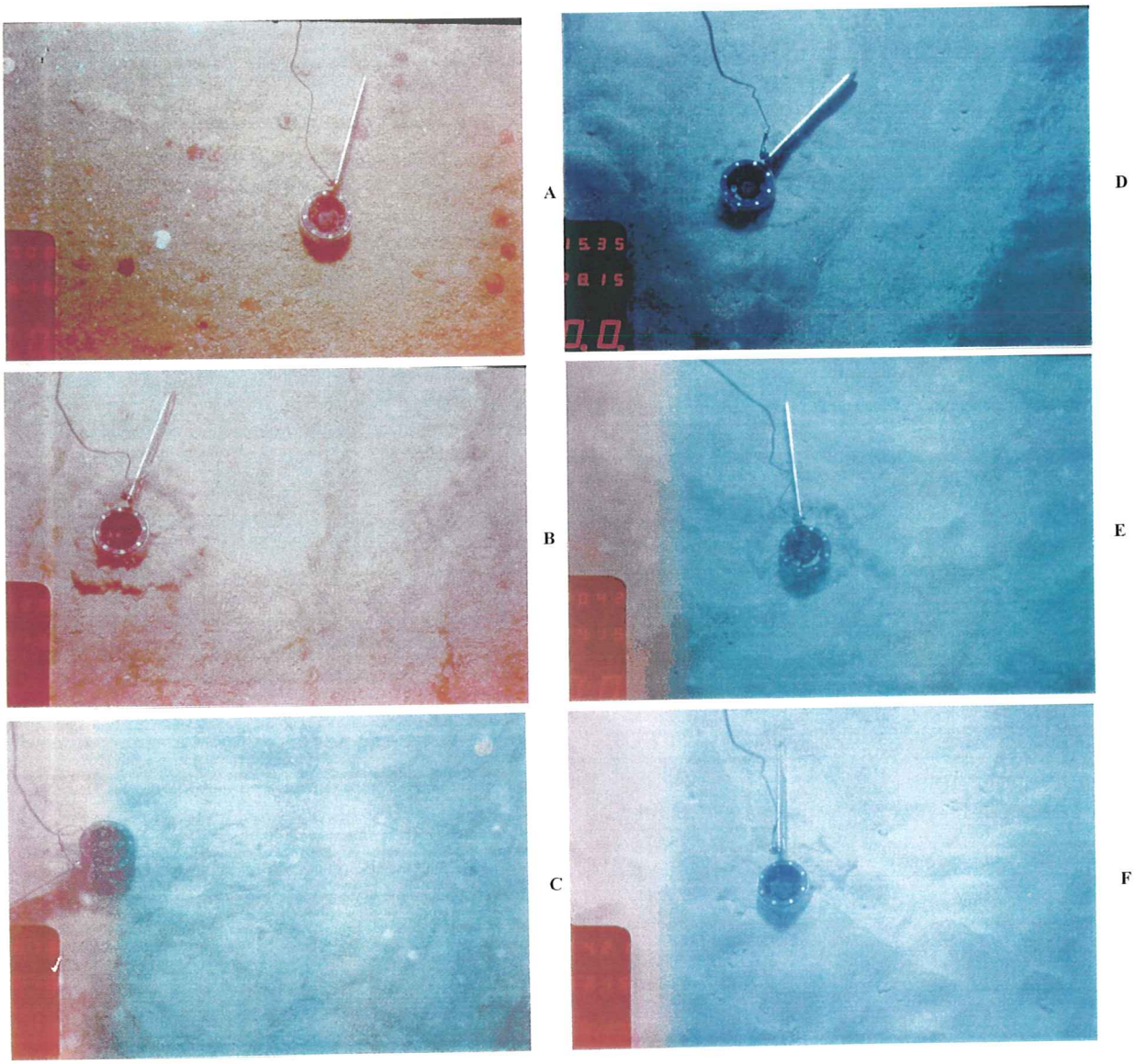

Fig. 3-14 Seabed photos collected along CoPan2 transect demonstrating ripple distribution across sand ridges on Sable.

of the storm and a return to fair-weather shelf conditions. Fig. 3-15 displays the images of resin peels collected along CoPan1 sand-ridge profile. Overall, HCS and cross bedding are more common on the western (stoss) flanks while parallel-low angle laminations often occur on sand ridge crests. At the CoPan site, HCS are also smaller and occur less frequently along the deeper CoPan2 profile than that along the shallower CoPan1 profile.

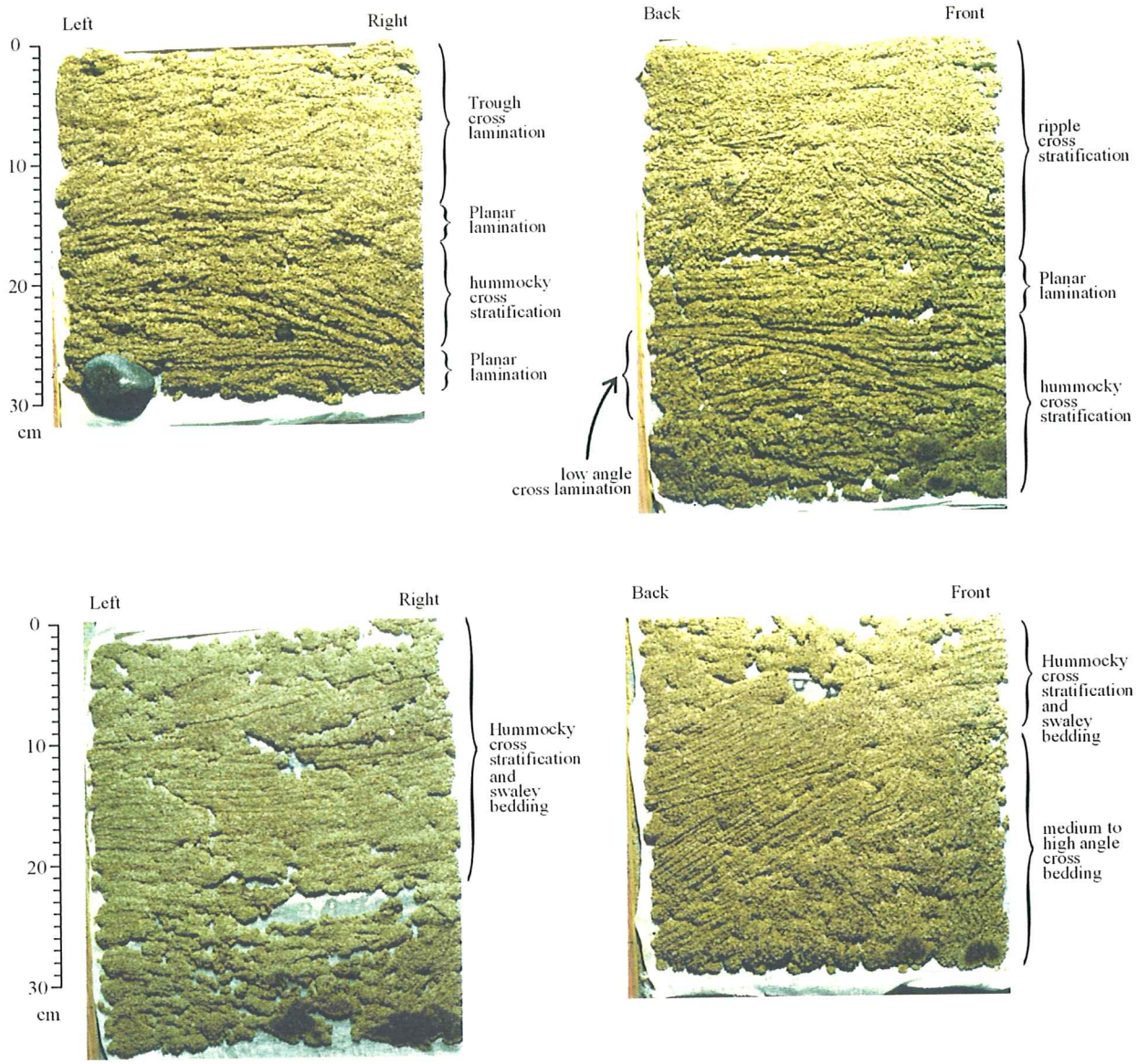

Fig. 3-15 Images of resin peels collected along CoPan1 sand-ridge profile demonstrating various shallow subsurface sedimentary structures. The arrows point the top of the IKU sample. B (back), F (front) indicate back and front, and R (right), L (left) indicate right and left relative to the ship's orientation. Upper: station 47, lower stoss-side location. Lower: station 50, mid stoss flank.

Fig. 3-15 (continued) Upper, sand ridge crest of station 51; Middle, mid-lee flank of station 33; Bottom, lower lee flank of station 28.

4. MIGRATION AND STABILITY

4.1 Sand Ridges and Sand Waves

The migration of sand ridges and their associated bedforms is a critical issue for the design and siting/routing of offshore platforms and pipelines as the migration of these bedforms can produce thick mobile sediment layers (Li et al., 1999). Previous studies arrived at different estimates of the sand ridge migration rates ranging from very little movement (Ingersoll and Ryan, 1997) to 50 m/yr (Dalrymple and Hoogendoorn, 1997). These findings are questionable because of the lower navigational resolution and density in the data used. The longer, state-of-the-art serial multibeam surveys generated in this project now enable us to derive more reliable estimates of sand ridge migration on Sable Island Bank.

Two methods are used in this study to determine the stability of large-scale bedforms using the repetitive multibeam surveys: serial comparisons of (a) trough line traces in map view and (b) trough-crest positions in profile view. The serial comparisons span from 1996 to 2000. Due to errors and uncertainties in sound velocity corrections, tidal predictions, and ship and system configurations, only vertical differences greater than 20 cm and horizontal differences over 10 m are believed to represent real morphological changes (King, 2002). In the map view method, tracings of trough lines on georeferenced multibeam images from each survey year were overlain to determine the rate and direction of sand ridge migration. The traced sand ridge and sand wave trough lines from the central repetitive survey area of CoPan are compared in Fig. 4-1. The shaded relief image of the central repetitive survey area is shown in the upper left diagram with the detailed comparison area being framed out in the box. The three zoomed panels show traced trough lines comparing the 1996 to 98, 1998 to 2000 and 1996 to 2000 time spans respectively. Fig. 4-1D demonstrates that sand ridges in the CoPan area had migrated up to 30 m from 1996 to 2000. This would convert to about 7 m/year migration rate for this time span. However, the 1998-2000 surveys (inset in Fig. 4-1C) indicate that maximum migration up to 15 m can occur in a single winter season. Fig. 4-1 also shows that traced sand ridge trough lines often criss-cross each other and thus suggests that the same sand ridge could have migrated in opposite directions at different points along its crest line. A more consistent migration pattern is found for the sand waves at CoPan: sand waves have generally migrated to the southeast for all three comparison periods and the maximum migration rate reached about 15 m/year. Some sand waves appear to have rotated anti-clockwise from 1997 to 98 (SW1 and SW2 in Fig. 4-1B). The traced sand ridge and sand wave trough lines from the

Fig. 4-1 Serial comparison of digitized sand ridge and sand wave trough lines for the CoPan area.

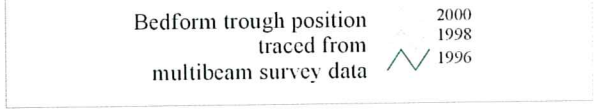

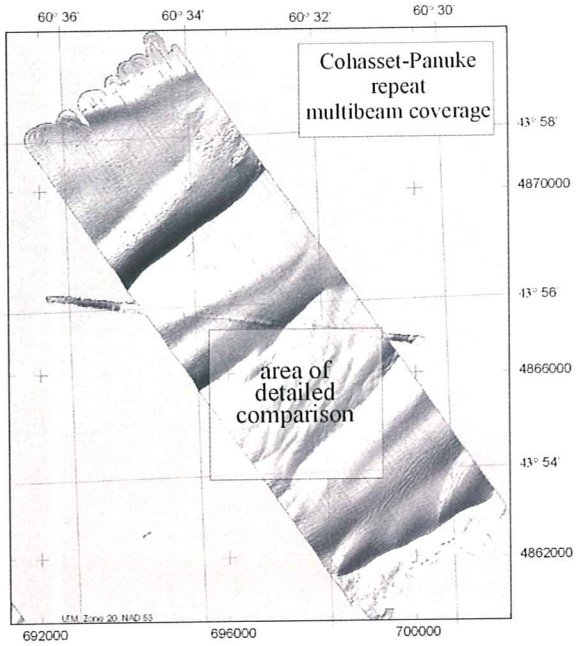

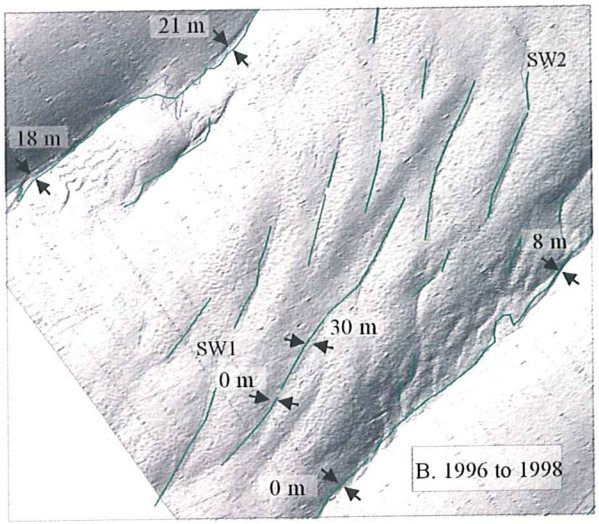

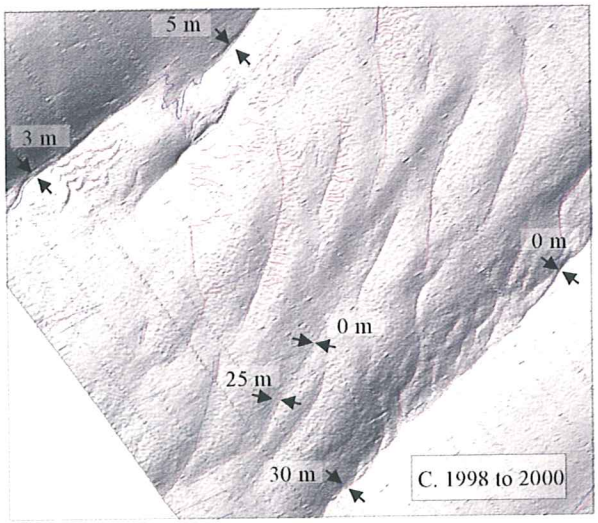

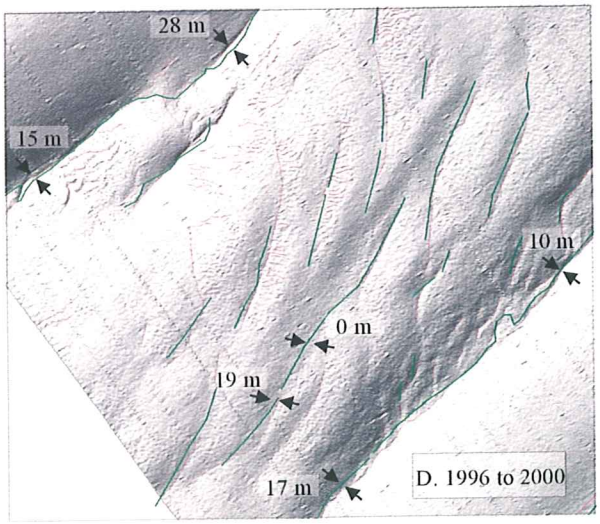

South Sable area are compared in Fig. 4-2. The 1997 to 98 serial comparison (Fig. 4-2B) indicates that sand ridges migrated up to 20 meters to the northwest. But during the period of 1998 to 2000 (Fig. 4-2C), sand ridges reversed the migration direction and moved to the southeast for maximum distances up to 30 meters. The opposite migrations in the 1997-1998 and 1998-2000 periods offset each other to result in nearly neutral to weak net southeastward migration over the entire 3 year time span (Fig. 4-2D). As for the CoPan area, sand waves at the South Sable area are also found to be more mobile with maximum migration rate reaching nearly 30 m/year. There is also a strong spatial variation of sand wave migration pattern. For instance, a group of five sand waves at the SE corner of the detailed comparison area (G1 in Figs. 4-2B and C) show a similar pattern of migration as the sand ridges: net migration to the northwest from 1997 to 1998 yet a net movement to the southeast from 1998 to 2000. However, a second group of sand waves immediately above the image center (G2 in Figs. 4-2B and C) showed the opposite pattern: they migrated to the southeast in the 1997-98 surveys but to the northwest from 1998 to 2000 surveys. They also seemed to have rotated clockwise during this process.

In the profile analysis method, the vertical profiles from different surveys along a transect were overlain and the shifts of sand ridge troughs and smaller bedform crests and troughs were used to estimate the migration rate and direction of sand ridges. The vertical profiles along the central repetitive survey area of CoPan are superimposed in Fig. 4-3. This profile comparison indicates that little change occurred between the 1996 and 1998 surveys along this particular transect. Moderate changes occurred from 1998 to 2000 and the difference is predominantly a 60-70 cm vertical accretion from 1998 to 2000. For South Sable area, profiles along two lines have been obtained from the 1997 and 2000 surveys and they are compared in Fig. 4-4 respectively (profile locations marked as thin red lines in Fig. 3-1). Profiles from the northwest corner (Fig. 4-4a) show that although the western flanks do not show clear migration, the eastern flanks and the superimposed sand waves have migrated 30-40 m to the east from 1997 to 2000. Fig. 4-4a also demonstrates up to 30 cm aggradation in the sand ridge troughs and on the eastern flanks during this time span. The profiles obtained along the line in the southeast corner are stacked in Fig. 4-4b. Again the profiles of the western flanks do not show clear net shift. Though one eastern flank shows crossing profiles, the superimposed sand waves and eastern sand ridge flanks show consistent eastward migration ranging from 15 to 50 m for the three year span of 1997 - 2000. Depending on the location on the transect, the seabed could have been eroded up to 0.3 m or aggraded to a maximum of nearly 1 m.

Comparisons in Figs. 4-1, 4-2, 4-3 and 4-4 are only for several selected sand ridges, and comparisons for

Fig. 4-2 Serial comparison of digitized sand ridge and sand wave trough lines for the South Sable area.

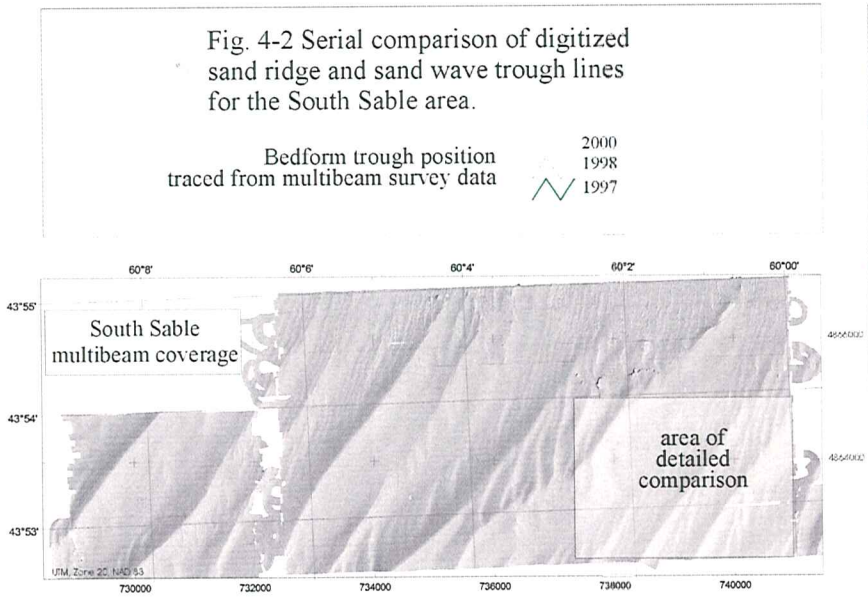

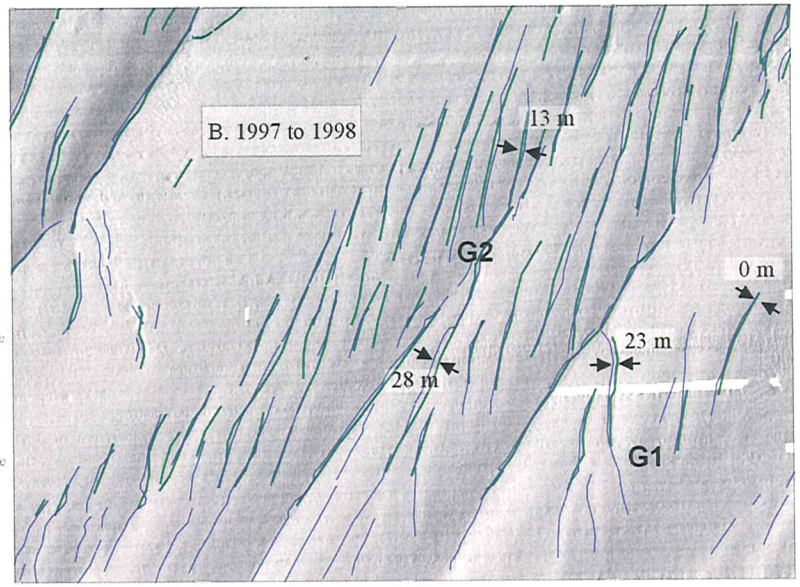

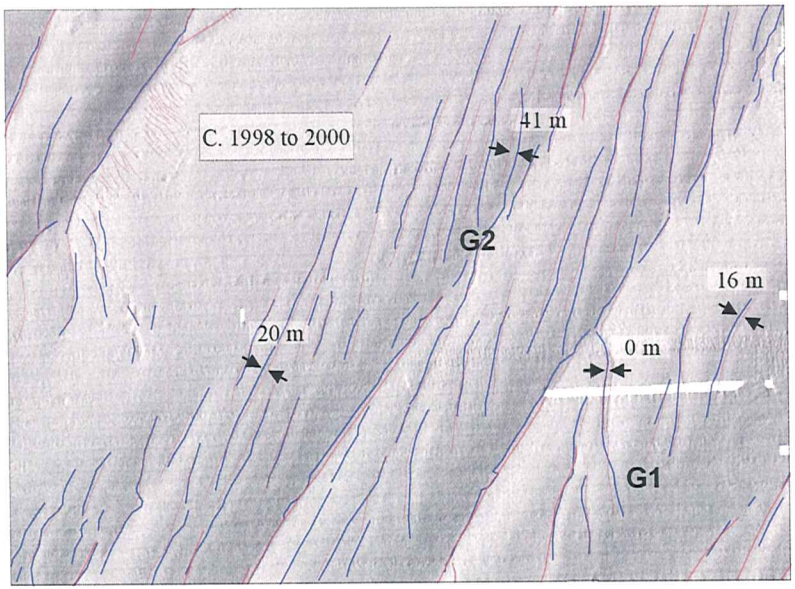

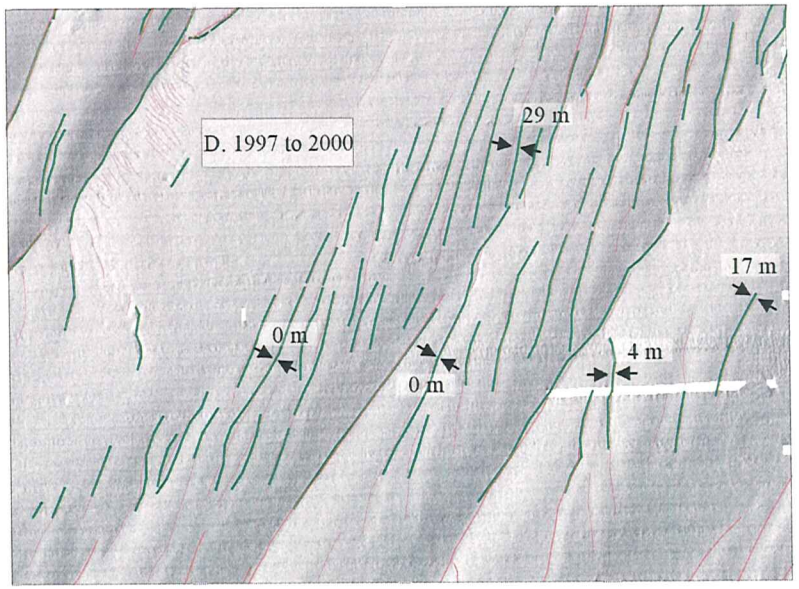

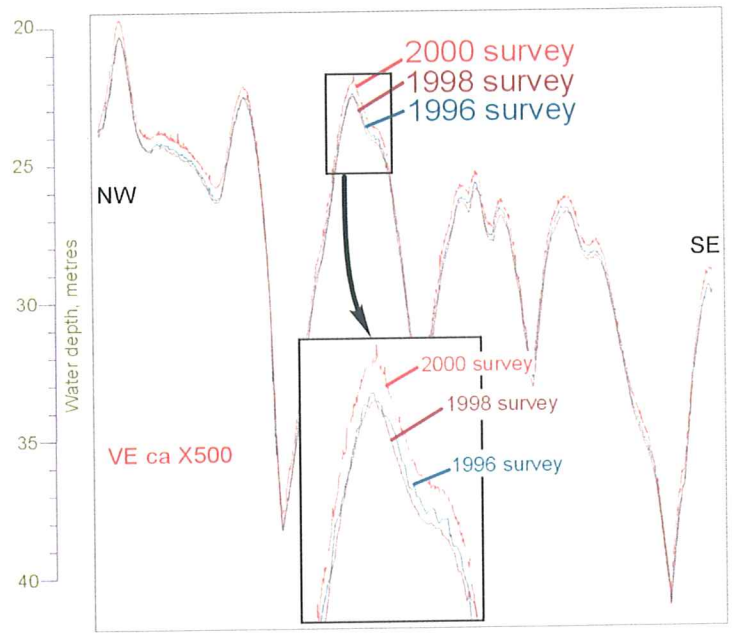

Fig. 4-3 Comparison of the vertical profiles from the 1996, 1998 and 2000 surveys across the CoPan central repetitive survey area.

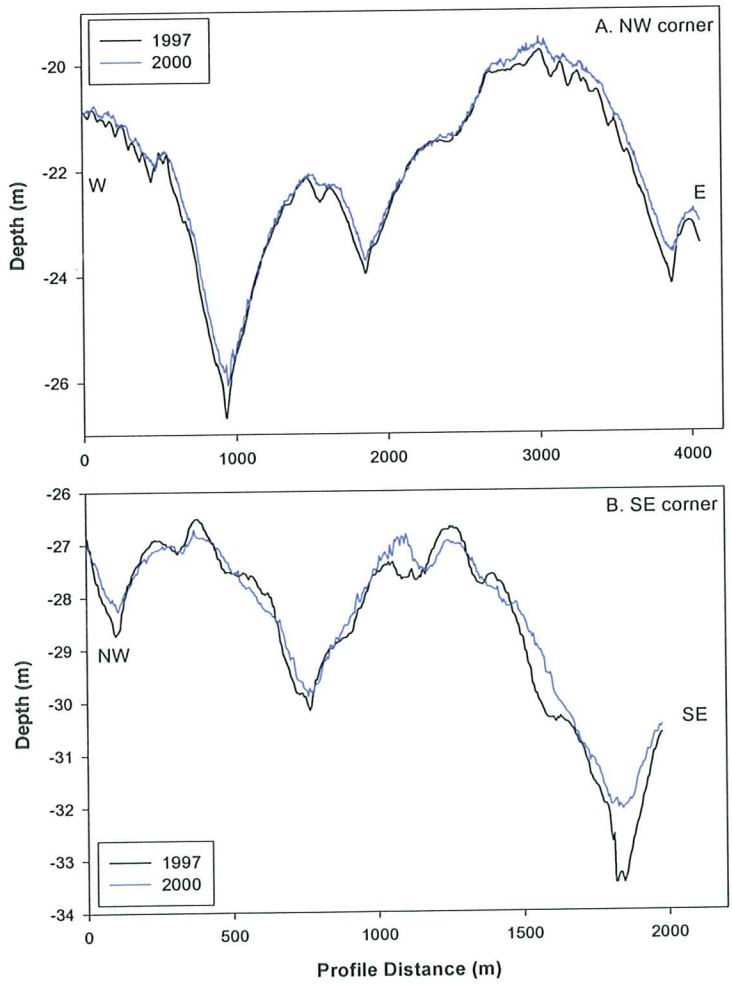

Fig. 4-4: Comparison of vertical sand ridge profiles from the South Sable area. Locations of profiles are shown as thin red lines in Fig. 3-1.

large populations of measurements are needed to derive statistically meaningful estimates of sand ridge migration rate and direction. Such an approach could also help identify and negate the numerous positional and vertical accuracy errors inherent in the multibeam data. A total of 26 transects at 150 m spacing across the CoPan area and 22 transects at 100 m spacing across the South Sable area were analyzed. Along each transect, serial profiles were overlain and the offset in both water depth and the location of all bedform troughs and crests were measured. In this way a large number of measurements (>400) over each serial survey area could be analyzed. Fig. 4-5 shows histograms of sand ridge migration rates based on vertical profile measurements for the CoPan area. For each pair of compared surveys, sand ridge migrations up to 50 m have been observed and they occur in both "stoss" (northwesterly) and "lee" (southeasterly) directions. The histogram curves indicate a mode of easterly migration from 1996 to 1998, but a mode of westerly migration from 1998 to 2000. When migration rates are averaged over the entire four year span, these opposite migrations tend to offset to result in nearly zero net sand ridge migration over longer time spans (purple line in Fig. 4-5). Migrations exceeding 30 m over a two year time frame represent only 5% of the measurements for the easterly migration and 10% for the westerly migration. Histograms of sand ridge migration rates based on profile measurements for the South Sable area are presented in Fig. 4-6. Again all three frequency distribution curves show that sand ridge migrations reached up to 50 m and occurred in both easterly and westerly directions. Migrations exceeding 30 m over the 1 year and the 2 year survey spans are less than 5% of the measurements. The difference from the CoPan site is that the modes of the distributions from all three time intervals are nearly neutral, with only weak bias towards westerly migration.

Comparisons of vertical profiles and traced trough lines from repetitive multibeam data, as demonstrated in Figs. 4-1 to 4-6, clearly show that sand ridges on SIB migrate at very low rates (mostly less than 20 m/yr, average around 5 m/yr) under present-day storm and tidal conditions, but the migration can be in opposite directions on shorter periods of time to result in no net migration over longer time spans. For the same time period, the migration direction can even be reversed at different points along a sand ridge crest line. Sand waves, superimposed on sand ridges, are found to be more active and their maximum migration rate can reach 30 m/year. The systematic, long term (millennium scale) eastward migration indicated by internal prograding strata in deeper water sand ridges (Dalrymple and Hoogendoorn, 1997; King, 2002) is not expressed in the annual to decadal observations here.

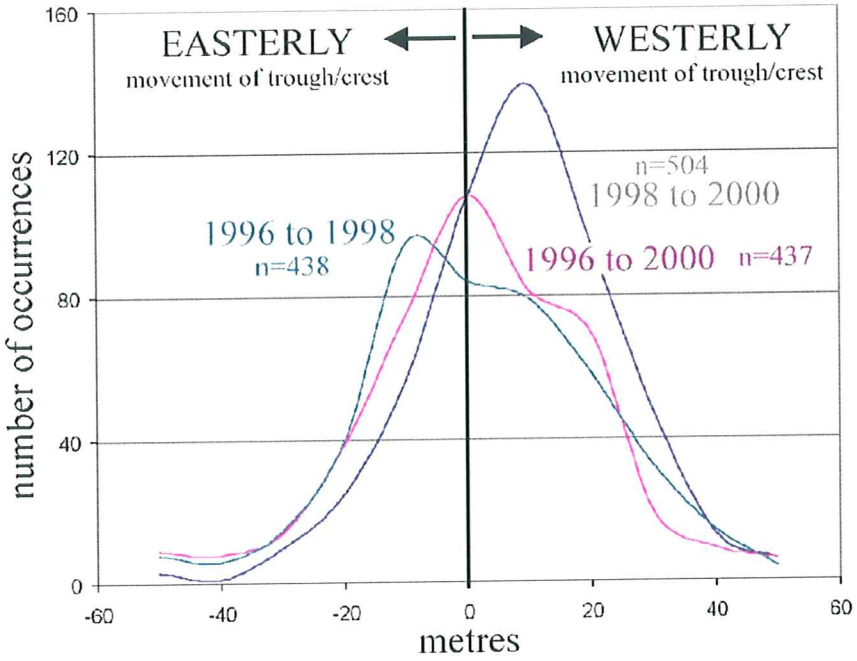

Fig. 4-5 Histograms of sand ridge migration measured from profiles for surveys 1996-1998, 1998-2000 and 1996-2000 for the CoPan site. n indicates the number of measurements for each serial comparison.

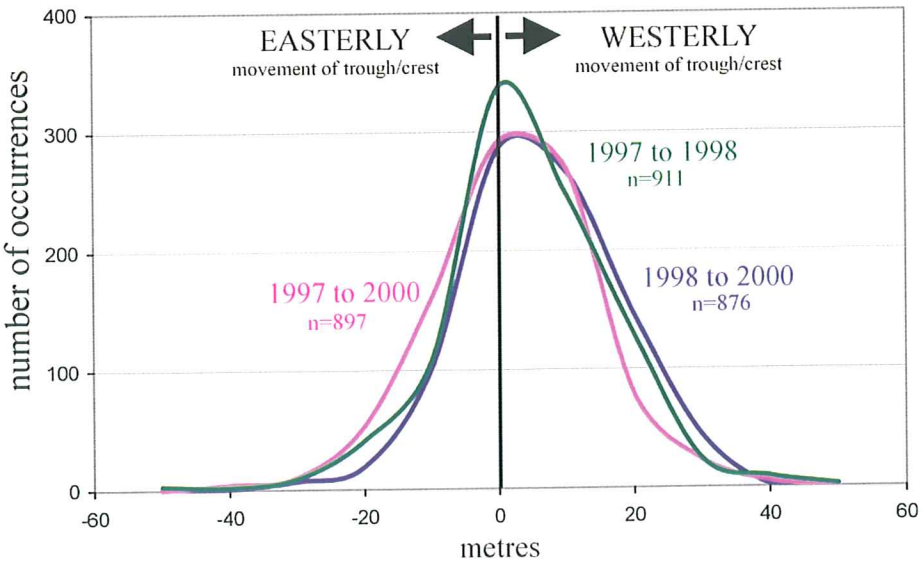

Fig. 4-6 Histograms of sand ridge migration measured from profiles for surveys 1997-1998, 1998-2000 and 1997-2000 for the South Sable site. n indicates the number of measurements for each serial comparison.

4.2 Mobility of Megaripples and Large Wave Ripples

Sidescan images collected along sand ridge transects have shown the superposition of megaripples and large wave ripples on sand ridges and sand waves (Figs. 3-7, 3-8 and 3-11). As these smaller bedforms tend to be more active during storms and their migration can produce mobile sediment layers up to 1-2 meters thick, it is important to understand their relationship with sand ridges and their mobility during storms. Fig. 4-7 depicts sidescan images obtained in October 2000 and May 2001 respectively from the Defence Research & Development Canada (DRDC) sediment acoustic property test site located about 45 km to the west of Sable Island in 70 m depth of water (courtesy of John Osler, DRDC Atlantic). The patches defined by sharp boundaries at the lower-left corner and lower center of each images are rippled scour depressions (RSD) which are covered by well-developed large wave ripples (LWR). The NE-SW trending linear features delineated by thin straight lines are sand ribbons. The coarser sediment on the bottom of the sand ribbons often show NW-SE oriented megaripples (upper image in Fig. 4-7). Comparison between the upper and lower images in Fig. 4-7 shows that the megaripples on the sand ribbon bottom and immediately to the left of the nadir survey track clearly recognized in the 2000 survey have disappeared in the 2001 survey and with this, minor shifts of the boundaries of the sand ribbons have also occurred. Though the rippled scour depressions persisted, the LWR within them have changed wavelength and orientation from 2000 to 2001over a single winter storm season. Subsequent GSCA sidescan surveys in 2002 (Miller et al., 2003) have detected further, but more subtle changes (Crawford, et al., 2002). This demonstrates that large wave ripples, megaripples and sand ribbons can be reactivated during typical winter storms, even in 70 m water depth. Repeat sidescan surveys in 1996 and 2000 along a shore-parallel transect in the shallow water (20 m depth) of South Sable have also demonstrated largely unchanged sand ridge troughs yet reactivation of linguoid megaripples and large wave ripples (Li et al., 2001b). Repetitive sidescan surveys along sand ridge transects at the CoPan and South Sable sites have also been collected on a 2002 Hudson expedition (Miller et al., 2003). These repeat surveys, in combination with sampling, repeat multibeam surveys, and in situ monitoring, will be correlated with storm data to evaluate the distribution, geometry, mobility and resultant mobile sediment layers of targeted bedforms on Sable Island Bank. This will constitute one of the short-term seabed stability research thrusts at GSCA.

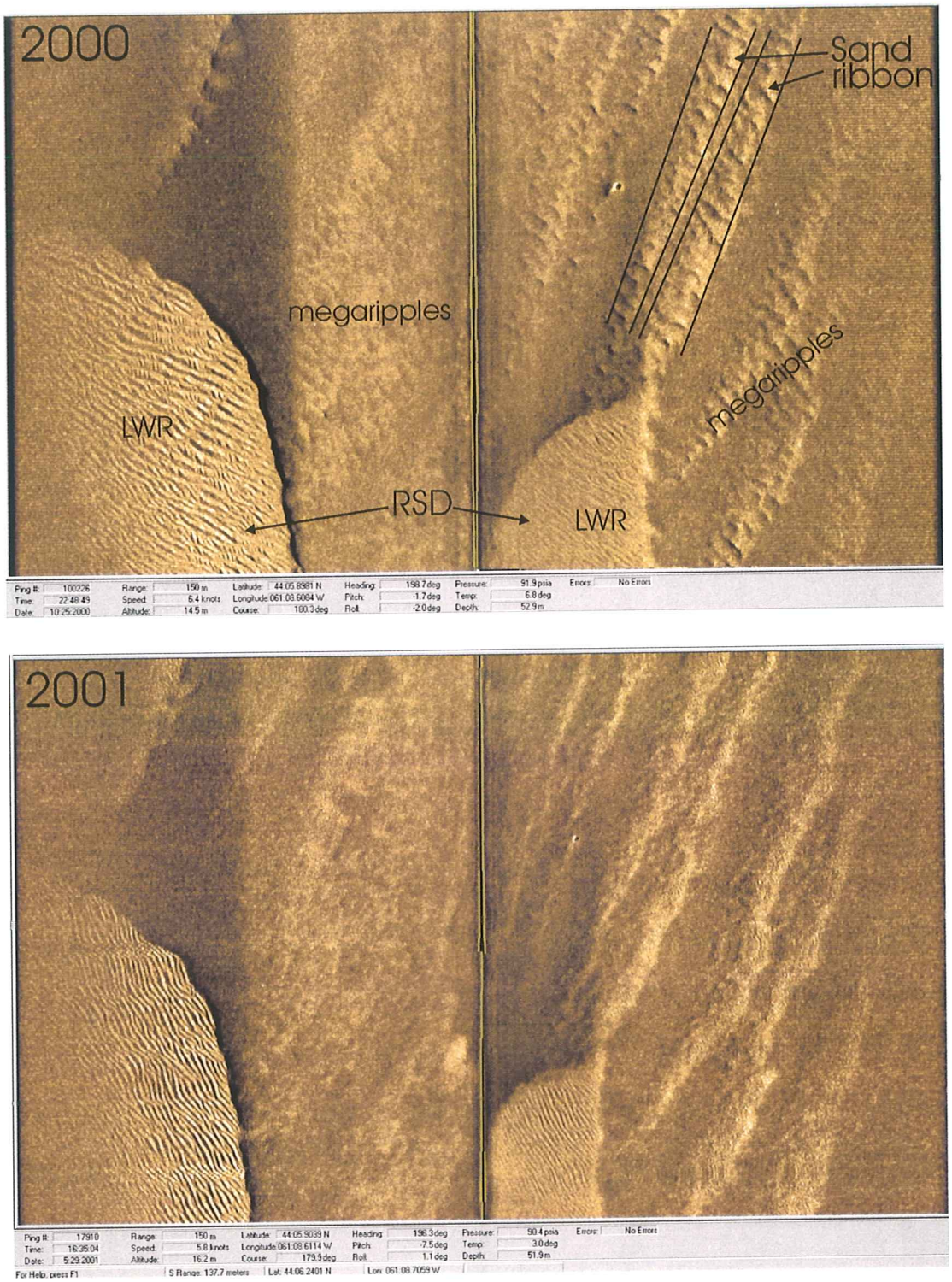

Fig. 4-7 Repetitive sidescan images obtained in 2000 and 2001 from the DRDC sediment acoustic property test site. (Courtesy of John Osler; Dark tones represent weak signal returns in contrast to other sidescan images in this report.)

5. HYDRODYNAMIC AND SEDIMENT TRANSPORT PROCESSES

As another component of this project, the GSC instrumented platform RALPH and S4 wave-current meters have been deployed along sand ridge transects to simultaneously measure nearbed wave-current dynamics and sediment transport processes during storms. The aim is to help identify the dynamic processes which may control or affect the morphology and migration of the sand ridges on Sable Island Bank. RALPH and two InterOcean S4 current meters were deployed along a sand-ridge transect at CoPan from January 17 to March 21, 2001 (see Fig. 3-9). RALPH was deployed on the sand ridge crest and the two S4 meters were deployed on the mid-eastern flank and in the western sand ridge trough respectively. Unfortunately the S4 meter in the ridge trough failed to collect any data, though RALPH and the S4 meter on the mid-stoss obtained simultaneous wave-current and sediment transport data (Smyth, 2001).

An image of the recently upgraded GSC instrumentation platform RALPH is shown in Fig. 5-1, with the S4 meters in the background. The key sensors on RALPH included a pressure transducer for depth/wave measurements, 4 electro-magnetic current meters (EMCM) and 2 acoustic Doppler velocimeters (ADV; not equipped in 2001 deployment) for current profile measurements, 6 optical backscatter sensors (OBS) for suspended sediment concentration measurements, 2 acoustic backscatter sensors (ABS) for bed elevation and sediment concentration profile measurements, 2 sector scanning sonars as well as a digital video camera to monitor seabed scouring and bedform development on the seabed. The S4 meter measured the wave and current speed at approximately 50 cm above the seabed. A single OBS with a data logger was also attached to the S4 to measure sediment concentration at 50 cm height. For this deployment, RALPH was programmed for sampling a 15 minute burst at 5 Hz frequency every 2 hours, while the S4 meter was set up for burst sampling for 10 minute duration at 2 Hz frequency every 2 hours. RALPH recorded useful data from 17 January to 4 February while the S4 meter recorded much longer, until 21 March. Detailed information and data analysis are provided in Smyth (2001).

The time series of the mean current speed and significant wave heights recorded by RALPH and the S4 meter are compared in Fig. 5-2. While mean current for RALPH was measured at 70 cm above the seabed (u_{70}), that for S4 meter was at 50 cm height (u_{50}). If the current is measured at the same location, the lower measurement height for the S4 meter could slightly reduce the mean current speed but the reduction should be less than 10%. Fig. 5-2c shows that one spring tide and two neap tides occurred during this deployment and the tide range was up to 1.1 m in the spring tide. The inequality of the mixed

Fig. 5-1 An image of the recently upgraded GSC instrumentation platform RALPH with S4 current meters in the background.

semidiurnal tide on Sable is apparent: a larger tide range is generally followed by a smaller tidal range in the next cycle.

There were two major and six minor storms during the entire deployment (Fig. 5-2b). The two major storms, with significant wave heights H_s reaching 4-5 m, occurred approximately around year-day (YD) 22 and YD 32. The comparison of mean velocity in Fig. 5-2a shows that the mean current speed over the sand ridge crest is much higher than that on the stoss flank: peak mean current speeds on the crest reached more than 0.7 m/s while that on the mid-stoss were approximately 0.4 m/s. In agreement with Li et al. (1999), this data set again shows that the mean current was more likely reduced at the peaks of storms (e.g. around YD 22 and YD 32). Detailed current and wave information for the period YD 20 to 24 are plotted in Fig. 5-3 to further demonstrate the variation of mean current speed and direction during the first major storm. Two major peaks of mean current occurred in this period (Fig. 5-3b), respectively around YD 21 and YD 23 with peak u_{70} values of about 0.7 m/s. Comparison between u_{70} recorded by

RALPH and u_{50} of the S4 meter again shows that the peak mean currents on the ridge crest have been enhanced by nearly 100% from the mid-stoss. The directions of the peak mean currents were predominantly to the north and the mean current on the sand ridge crest only lagged slightly behind that on the mid-stoss (Fig. 5-3a). This implies that sediment transport and sand ridge migration, if any occurred, were to the north during this analyzed period. GSC sediment transport model SEDTRANS96 (Li and Amos, 2001) was applied for sediment transport prediction. The calculated total sediment transport rates on the sand ridge crest were 0.0145 and 0.0295 kg m^{-1} s^{-1} respectively for the two peaks of the mean currents in Fig. 5-3. The calculated total transport rates decreased to 0.00058 and 0.00303 kg m^{-1} s^{-1} at the mid-stoss site. This suggests that seabed erosion had occurred on the sand ridge crest and that sediment accretion probably occurred on the upper stoss side between the RALPH and S4 deployment locations.

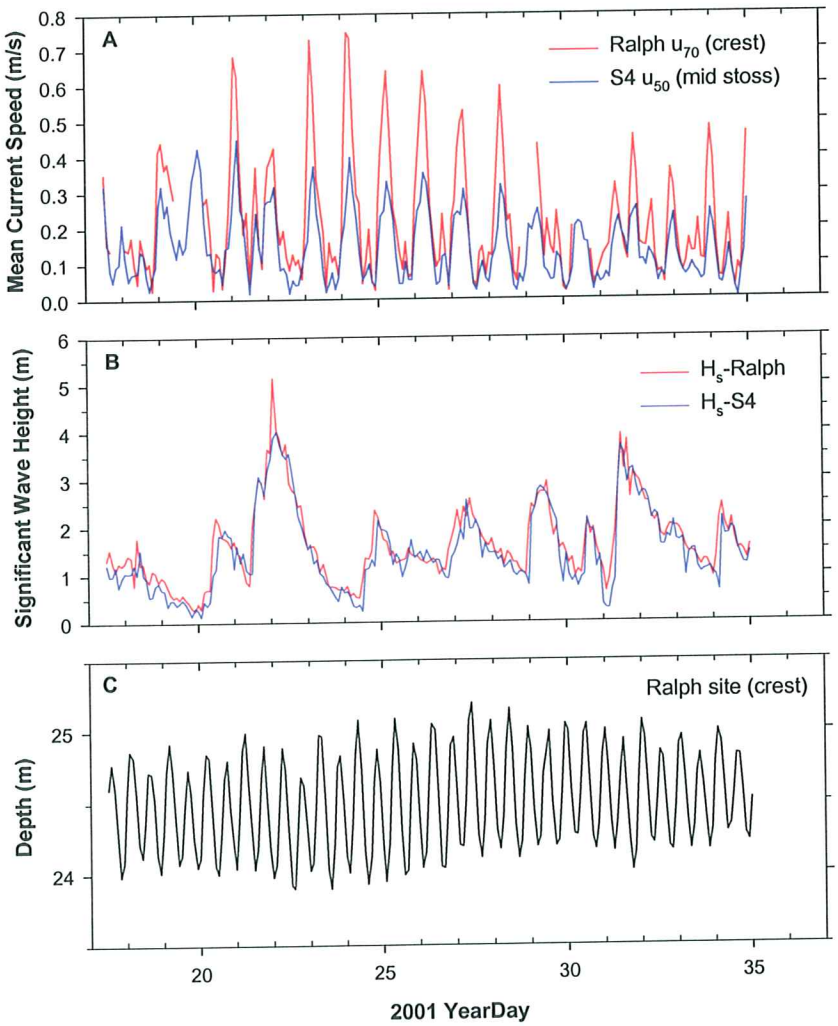

Fig. 5-2 Time series of the mean current speed and significant wave heights recorded by RALPH and S4 meter. The lower panel displays the depth data recorded by RALPH on the sand ridge crest.

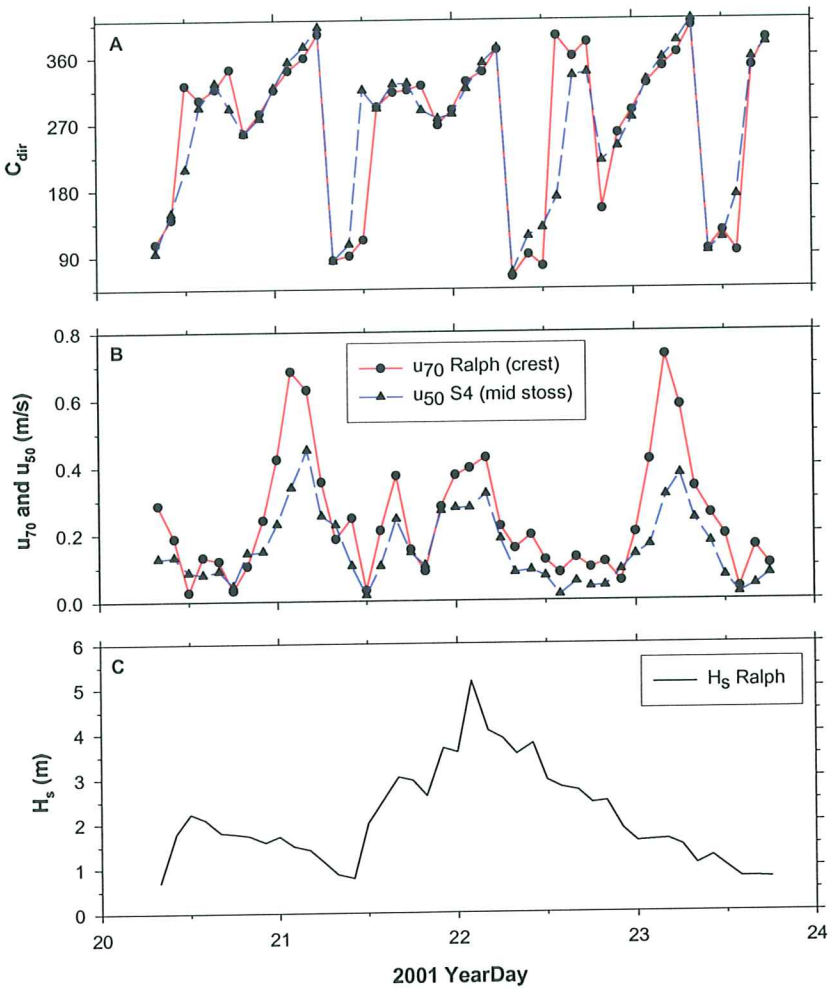

Fig. 5-3 Time series of (a) mean current direction, (b) mean current speed and (c) significant wave height for the period YD 20 to 24 from the 2001 CoPan1 deployment.

As storm-driven surface currents can reach up to 110 cm/s and are much higher than peak tidal currents (35-40 cm/s) on Sable Island Bank (Mobil Oil Canada Ltd., 1983; Hoogendoorn and Dalrymple,1986; Li et al., 1997), strong sediment transport events and hence sand ridge migration should mostly be determined by the magnitude and direction of the total mean current obtained from vectorial addition of the tidal and wind-driven currents during major storms. Fig. 5-4 shows the longer time series of significant wave height and mean velocity data recorded by the S4 meter on the mid-stoss site. Detailed wave and current information for the two major current events, marked by the two horizontal bars in Fig. 5-4, are further analyzed in order to elucidate the variation of peak mean current speed and direction during storms and its effect on sand ridge migration. Plotted in Fig. 5-5 are the time series of significant wave height H_s, wave propagation (toward) direction W_{dir}, mean current speed at 50 cm above seabed u_{50}, and the direction of mean current C_{dir} for the first event from YD 20 Hour 17 to YD22 H13. The waves

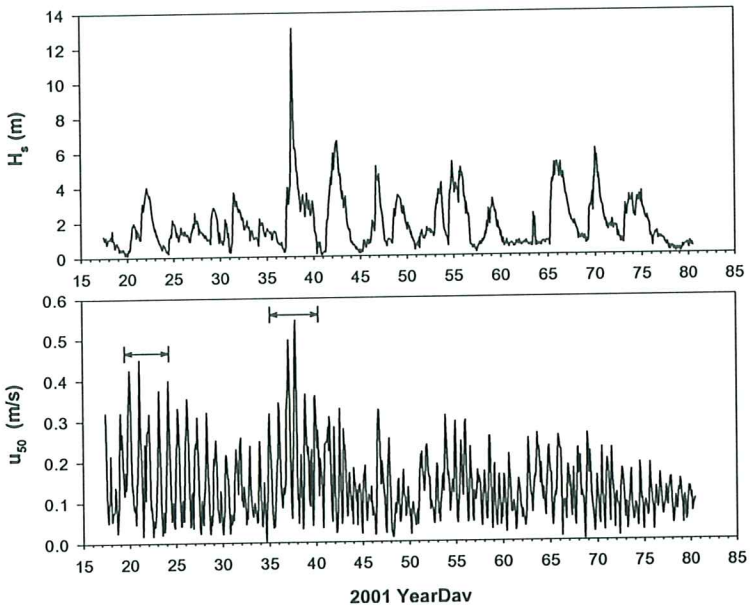

Fig. 5-4 Time series of significant wave height and mean current speed recorded by the S4 meter on the mid-stoss site from the 2001 CoPan1 deployment. Horizontal bars mark periods examined in greater detail.

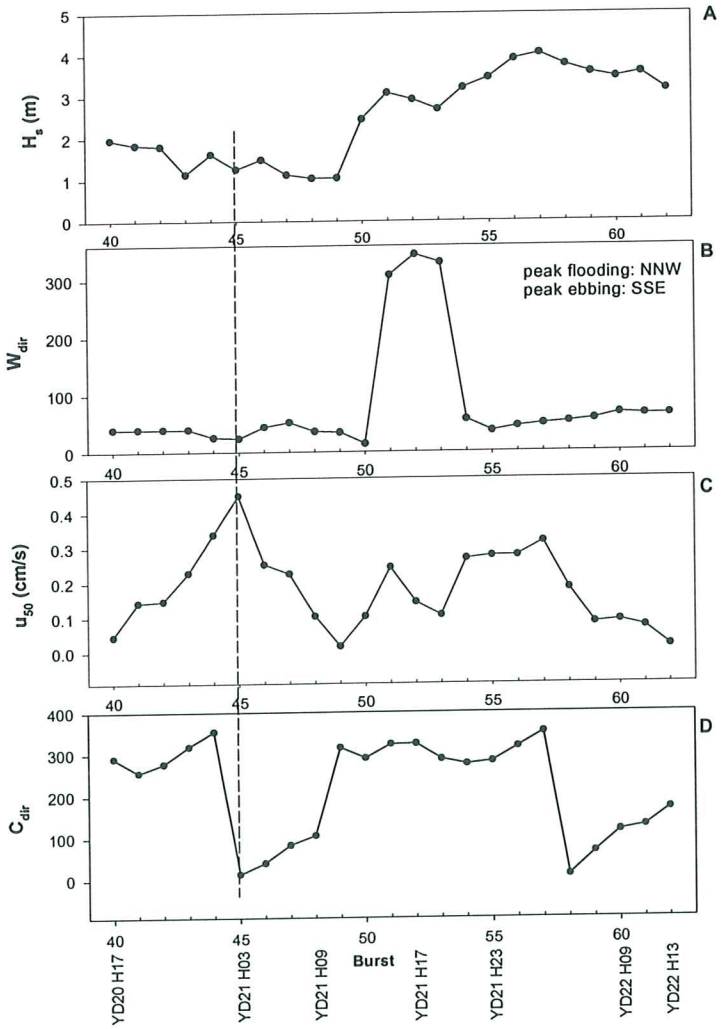

Fig. 5-5 Time series of significant wave height H_s, wave propagation (toward) direction W_{dir}, mean current speed at 50 cm above seabed u_{50}, and the direction of mean current C_{dir} for the period from YD 20 Hour 17 to YD22 H13 of the S4 data.

are assumed to be wind forced and the wave height and wave propagation direction are used here as indication of wind intensity and direction. For the dominant peak of mean current marked by the vertical dashed line in Fig. 5-5, effect of the wind was moderate (H_s around 1.5 m) and was to the NNE (24^0). The wind-driven current thus formed a small angle with the peak flooding tidal flow (to NNW). This led to effective vectorial addition between the peak flooding tidal and wind-driven current and the enhanced total mean current of about 45 cm/s predominantly toward the north (Figs. 5-5c and 5-5d). The implication is that sediment transport and hence sand ridge migration should be to N or NW for this event. Time series of similar detailed data for the event around YD37 have been plotted in Fig. 5-6. The dominant peak mean current in this event occurred at YD37 H21. Strong wind (H_s reached 12 m) was associated with this event but the wind was blowing to ENE (72^0). Thus the wind-driven current formed small angles with the peak ebbing tide (to SSE) and this resulted in a strong total mean current of 55 cm/s flowing to the SSE (163^0; Figs. 5-6c and 5-6d). This SSE peak total current presumably forced sediment transport and sand ridge migration to the SE during this second event. The conclusion drawn from analyzing these two events is that the peak total mean currents can be either to the northwest or southeast from storm to storm and thus sand ridges could migrate in opposite directions in different storms.

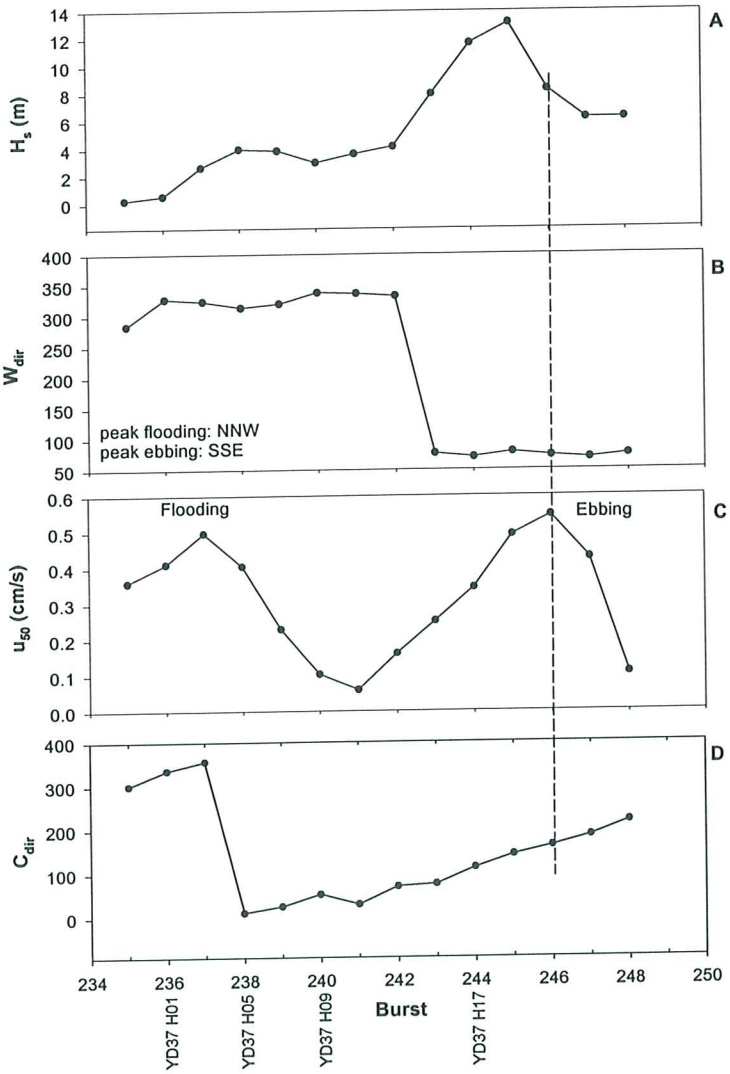

Fig. 5-6 Time series of significant wave height H_s, wave propagation (toward) direction W_{dir}, mean current speed at 50 cm above seabed u_{50}, and the direction of mean current C_{dir} for the period from YD 37 H01 to YD38 H01 of the S4 data.

6. DISCUSSION

6.1 Storm Processes and Ridge Migration

Comparisons of serial multibeam data spanning several years in Section 4 indicate that sand ridges on Sable Island Bank migrate at very low rates and the migration can be in opposite directions from survey to survey. Analysis of detailed current data from two storm events (Section 5) suggests that the peak total mean current from vectorial superposition of peak tidal current and wind-driven current can be to either the NW or SE to cause the observed migration of sand ridges in opposite directions. An understanding of the variation of wind-driven current during major storms and the historical storm track data is needed to further establish how storm process controls the sand ridge migration on Sable Island Bank.

According to Swift et al. (1985), Niedoroda et al. (1985) and Hoogendoorn (1989), the sand ridges on Sable are mainly under the influence of a friction-dominated zone during significant winter storms (wind speed approximately 25 m/s). Under this condition, the surface frictional layer (the surface Ekman layer, Ekman, 1905) occupies the entire water column and the wind-driven current near the seabed is roughly parallel with the wind direction. Two common scenarios of storm track are depicted in Fig. 6-1. The storm path lies to the northwest of Sable Island (Fig. 6-1A) in the first scenario. The storm low-pressure centre lies to the southwest of the Island at the early stage of the storm. Wind and hence the wind-driven current will be to the NW or N to cause northwesterly-directed sediment transport and ridge migration. At the peak and waning stages of the storm, the storm center will be located to the northwest and north of the island respectively. Wind and hence the wind-driven current will be to the NE and then rotate through the east to southeast. This will result in southeasterly-directed sediment transport and sand ridge migration (assuming predominance of wind-driven current over tidal current). Therefore sediment transport and ridge migration can switch from northwesterly directed to southeasterly directed through the course of a single storm but the dominant ridge migration at the storm peak will be eastward. In the second scenario, the storm path lies to the southeast of the Island (Fig. 6-1B). In this situation, the storm centre lies to the south, southeast and northeast of the Island at the early, peak and waning stages fo the storm respectively. The resultant sediment transport and ridge migration changes from westerly and southwesterly directed, to southeasterly directed through the course of a single storm in the second scenario, but the dominant ridge migration will be westward at the peak of the storm.

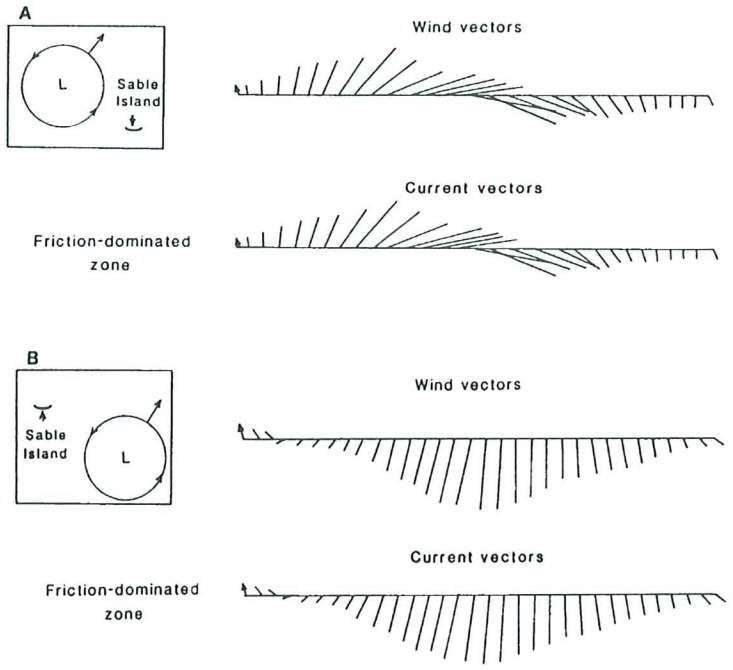

Fig. 6-1 Schematic representation of the wind and bottom current vectors in the friction-dominated zone in response to (A) a storm that passes to the northwest of the Sable Island and (B) a storm that passes to the southeast of the Island (modified after Hoogendoorn, 1989).

Based on the storm catalogue of Lewis and Morgan (1984), a total of 125 storms with wind speeds greater than 25 m/s occurred on the east coast of Canada over the period from 1957 to 1983. Of these storms, 48% passed to the north of the Island, 33% passed to the south and the remaining 19% passed over the Island. This historical storm data suggests that the percentage of storms passing to the south of the Island is only slightly lower than those passing to the north of the Island. As the dominant sand ridge migration is to the east for storms passing to the north of the Island and to the west for storms passing to the south, the long-term storm statistics thus determines that sand ridges on Sable Island Bank may migrate to opposite directions in short time scales but net migration averaged over longer time spans should be very low with a slight bias to an easterly net migration. This is consistent with observations.

6.2 Sediment Mobile Layer Depth

Sediment mobile layer depth is a critical criterion in determining the routing and burial depth of offshore

pipelines and cables. The more accurate estimates of bedform metrics and migration rates obtained in this study can be translated into better prediction of sediment mobile layer depth during storms on Sable Island Bank.

Comparisons of repetitive multibeam surveys have established that the maximum observed bedform migration for the various survey spans is 50 m and that migrations exceeding 30 m represent under 10% of the bedform migration measurements (Section 4 and Figs. 4-5 and 4-6). Based on the bedform metric data in Table 1, the average sand ridge flank slope is approximately 0.0064. For 30 m migration of average sized sand ridges, the mobile layer depths will be less than 0.2 m. If we assume the average steepness of equilibrium sand waves is 0.01, then 90% of mobile layer depths generated by sand wave migration should be less than 0.6 m. These average values are in good agreement with estimates based on in situ RALPH measurements (Li et al., 1999) and IKU grab core peels (Hudson Cruise 96029 report). The steepest sand ridges in the survey areas have a flank slope of 0.0184 (2 x maximum steepness 0.0092 in Table 1). With the maximum measured migration of 50 m, this converts to a maximum mobile layer depth of 0.9 m. As for sand waves, their steepest flank slope is 0.024 (2 x maximum sand wave steepness in Table 1) and thus the thickest mobile layers generated by sand wave migration will be about 1.2 m. These estimated maximum mobile layer depths are coincidently very close to the maximum 1 m vertical erosion/aggradation shown by the profile comparisons in Fig. 4-4. They are also in agreement with the maximum thickness of the master bedding units (Dalrymple and Hoogendoorn, 1997) and event bed thickness estimates from vibrocores (King, 2002) and cone penetrometer data (Forsythe, 1998).

6.3 Bedform Symmetry Variation with Depth

Morphological data given in Section 3.1 indicate that there is a general transition of sand ridge symmetry from slightly asymmetrical to the west in the shallow water to asymmetrical to the east in the deep water. Sand waves superimposed on sand ridges also show opposing profile asymmetry on the opposite flanks of sand ridges. Is there an overall trend of bedform symmetry with water depth? If so, what processes have caused this?

Symmetry of sand ridges and sand waves at CoPan is plotted as a function of latitude (from shallow water to deep water) in Figs. 6-2A and 6-2B respectively. Firstly, at any given depth, bedforms are asymmetric to either east or west. This is probably due to the fact that wind-driven current and sediment

transport can switch from northwesterly directed to southeasterly directed through the course of a single storm and that there are about equal number of major storms passing to the south versus to the north of the island. Analysis of RALPH and S4 data in Section 5 has shown that the mean current is strongly enhanced over the sand ridge crest and decreased greatly on the downstream flank due to flow relaxation in the sand ridge trough. Thus when the peak total current is toward the eastern sector (northeast to southeast), it accelerates on the western sand ridge flank and decelerates on the eastern flank. Conversely, the peak total current flowing to the western sector would result in enhanced current on the eastern sand ridge flank and reduction on the western flank. Therefore the western ridge flanks are dominated by eastward storm-generated flows and bedform migration, and oppositely the eastern sand ridge flanks are more affected by the westward storm flows and bedform migration. This differential effect might explain the observed opposing asymmetry of sand waves on the opposite flanks of sand ridges (Fig. 3-5).

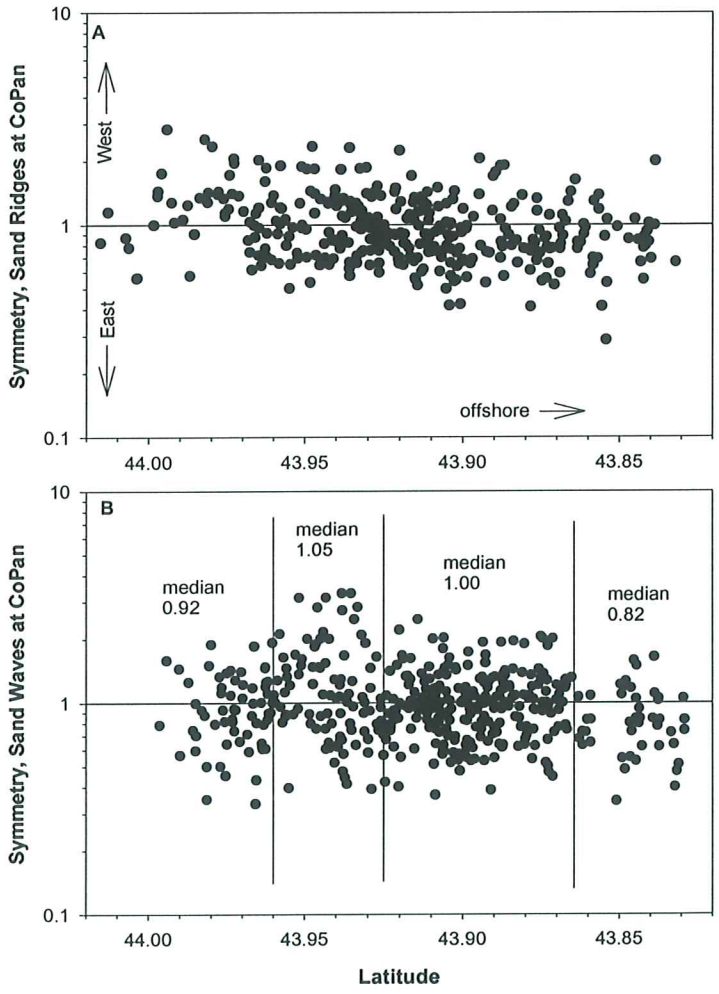

Fig. 6-2 Symmetry of (A) sand ridges and (B) sand waves at CoPan plotted as a function of latitude (from shallow water to deep water).

Despite the scatter, sand ridges at CoPan also show a trend of decreasing symmetry from nearshore to offshore (Fig. 6-2A). Sand ridges in the shallow water are generally asymmetric to the west and become predominantly asymmetric to the east in the deep water. Sand waves demonstrate a slightly different pattern (Fig. 6-2B). They show an overall asymmetry to the east in the shallow water, gradually become asymmetric to the west in the intermediate depths before finally becoming asymmetrical to the east again in the deep water. Sand ridges and sand waves at South Sable show similar but weaker trends. These patterns are probably caused by the coastal setup and development of downwelling currents during storms. Fig. 6-3, modified after Niedoroda et al. (1985), shows the schematic wind and current structure at the peak of a storm that passes to the northwest of Sable Island (the scenario most strongly affecting the study area). In the shallow depths, the on-shore wind component causes coastal setup and the pressure gradient drives an offshore directed bottom downwelling flow. As the downwelling flow advances offshore, the Coriolis force steers the flow to its right (to west) in the intermediate depths. This westerly-turned downwelling flow augments the westerly directed wind-driven flows at the early stages of storms so that sediment transport to the west is balanced with or stronger than sediment transport to the east. This causes the bedforms to be nearly symmetric or slightly asymmetric to the west in the shallow and intermediate depths (Fig. 6-2). Further offshore, the downwelling flow weakens and the seabed is dominated by the northeasterly-directed wind driven current. Therefore the bedforms become increasingly asymmetrical to the east in greater water depths. Alternatively, the symmetry variation with depth could be a result of the much longer-term effects of sea-level change and sand ridge evolution. Under post-glacial conditions of lower sea-level and abundant sand supply, stronger and predominantly eastward wind-driven flows during storms caused large sand volumes to be transported to the east as indicated by strong eastward migration of sand ridges in their early development stages. As sea-level rose, the hydrodynamic regime changed so that further development of sand ridge morphology was largely through erosion in the troughs and trough-parallel longitudinal lengthening rather than crest-normal lateral migration (King, 2002). This change in the sand ridge development process would not have the dominant eastward transport of earlier times, resulting in less marked sand ridge asymmetry. Under the raised sea-level, the deep-water sand ridges became less active yet their eastward asymmetry developed during their early formation stages was preserved.

6.4 Distribution and Generation of Gutters

The multibeam surveys conducted in this study have shown wide occurrence of shore-normal erosional

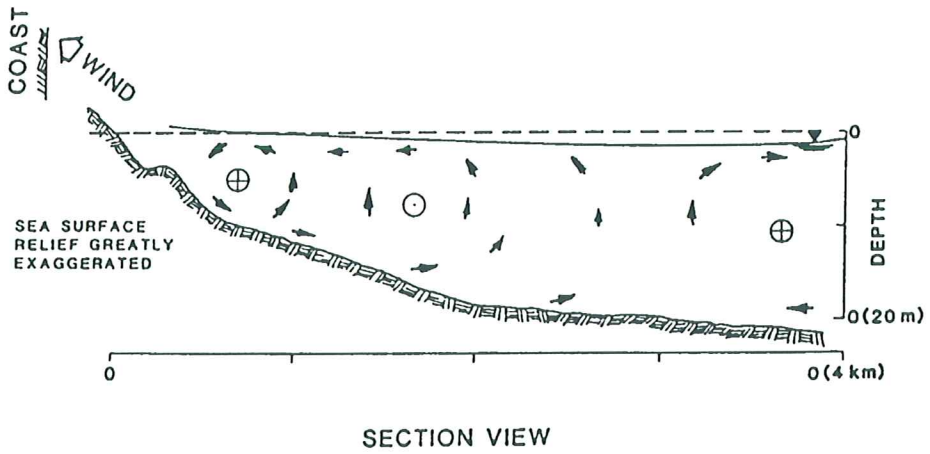

Fig. 6-3 Schematic showing the wind and current structure at the peak of a storm that passes to the northwest of the Sable Island. ⊕ indicates flows into the page and ⊙ indicates flows out of the page.

gutters at South Sable. These erosional channels are mostly restricted to water depths less than 20 m and are largely absent in the CoPan area. Analysis of the data from an earlier RALPH deployment (Amos et al., 2003) suggests that the coastal setup and the subsequent down-welling was responsible for the formation of smaller-scaled gutters on the shoreface of Sable Island Bank.

As depicted in Figs. 6-1 and 6-3, there would be an on-shore component of the wind at the early and peak stages of storms passing to the north of the Island. Similarly at the early stages of storms passing to the south of the Island, wind would be to the west and surface Ekman layer flow will be directed to the right (on shore) of wind direction. As Sable Island acts as a coastal barrier, coastal setup and hence offshore-directed downwelling bottom flow would occur in both cases to cause erosional offshore sediment transport and gutter formation in the South Sable area. Since the conditions favouring coastal setup and downwelling generation only last for a few hours during a storm, the gutter formation process should be short-lived. As the downwelling flow moves further offshore, it loses its power and wind-driven currents, mainly to the northeast or west, become dominant. Therefore the distribution of gutters is generally limited in depths shallower than 20 m. In the CoPan area, there is no island barrier to facilitate the coastal setup and downwelling generation. Thus gutters are absent in this area. Similar barrier effect on the downwelling current generation was also observed in the nearshore zone of the Canadian Beaufort Sea (Hequette, et al., 2001).

7. SUMMARY

(1) Serial multibeam bathymetric coverages spanning 1996-2000 have been obtained for the CoPan and South Sable areas on Sable Island Bank.

(2) These multibeam data demonstrate a series of NE-SW trending sand ridges. The average height and wavelength of sand ridges in the South Sable area are 3.5 m and 1.1 km respectively. Sand ridges in the CoPan area are generally bigger: their average height is 4.6 m and average wavelength is 1.7 km. The size of sand ridges tends to increase toward offshore. The majority of sand ridges are nearly symmetrical. Though there is strong local variation, sand ridges in the shallow water are generally asymmetric to the west and become predominantly asymmetric to the east in the deep water. This trend is probably caused by the coastal setup and development of downwelling currents during storms. Alternatively, it can be a result of longer-term rise in sea-level and progressive diminishing of eastward migration.

(3) Seabed sediment is composed of coarse sand in the trough and at the lower stoss (western) flank, and fines progressively eastward toward the sand ridge crest to change to fine sand on the crest and the lower lee (eastern) flank. Sediment on the sand ridge crest is best sorted and becomes slightly less well sorted toward the troughs. Under summer fairweather condition, the sand ridge troughs are characterized by a brownish, bioturbated bed covered by a thin layer of organic-rich fine sand. These give way to small current or wave ripples on the stoss or lee flanks. As wave and current effect becomes strongest on sand ridge crest, three-dimensional linguoid current ripples dominate on the crest.

(4) Resin peels from box cores reveal typical storm event bed structure: medium to high-angle cross lamination/bedding of the lower portion of the peels changes to hummocky cross stratification (HCS) and/or swaley bedding in the middle section, which is in turn overlain by ripple cross stratification and parallel or low-angle cross bedding at the top of the peels. This sequence of structure reflects the development and migration of asymmetric megaripples, hummocky or low-relief megaripples, and normal ripples in the progress of a storm.

(5) Sand waves are superimposed on sand ridges with 20-30^0 anti-clockwise rotation from the sand

ridge orientations. The average height and wavelength of sand waves in South Sable area are 0.45 m and 130 m respectively. Sand waves in the CoPan area are on average 0.53 m high and 200 m in wavelength. The very low steepness ratios are interpreted as caused by post-storm degradation or alternatively by modification of longitudinal flow erosion. Sand wave asymmetry along selected profiles indicates opposite transport directions on opposing sand ridge flanks. This is attributed to the differential effects of the eastward and westward wind-driven flows and bedform migration on the opposing flanks of sand ridges.

(6) A hierarchy of superimposed bedforms are observed from the combined multibeam and sidescan data. Sand waves are superimposed on sand ridges. Megaripples develop in the troughs of sand ridges and sand waves. Large wave ripples are found superimposed in the troughs of megaripples or occur independently in the troughs of sand ridges.

(7) Shore-normal, linear to irregularly shaped, erosional gutters widely occur in depths shallower than 20 m on the shoreface in the South Sable area. They typically show v-shaped cross-profiles with very low relief, average spacing of 35 m and mean depth of 19 cm. Gutters are generally absent at the CoPan site. Coastal setup and offshore-directed downwelling during specific stages of storms are proposed for the formation and distribution of these erosional gutters.

(8) In situ hydrodynamics and sediment transport data collected simultaneously along a sand ridge transect show that both the mean and instantaneous current speeds are significantly enhanced on sand ridge crests causing possible erosion on sand ridge crests and accretion on upper ridge flanks. Depending on the relative directions between peak tidal currents and storm-driven flows, the peak total mean currents can flow either to NW or SE in different storms.

(9) Comparisons of repetitive multibeam data indicate that sand ridges migrate at very low rates (mostly less than 20 m/yr, average around 5 m/yr), but the migration can be to opposite directions at different points along their crestlines. Also the migration can be to opposite directions on shorter periods of time to result in no net migration in longer time spans. Sand waves are found to be more active and their maximum migration rate can reach 30 m/year. Analysis of the variation of wind-driven current direction during a storm and the historical storm track data suggests that the switch of wind-driven current and sediment transport from northwesterly directed to southeasterly directed

through the course of a single storm, and the nearly equal number of major storms passing to the south versus to the north of the Island support the observed sand ridge migration pattern.

(10) Trigonometric calculations using the more accurate estimates of bedform metrics and migration rates obtained in this study show that migration of average sized sand ridges will produce mobile layers less than 0.2 m thick, while migration of sand waves produces mobile layers of 0.6 m. These values represent less than 10% of the measured sand ridge and sand wave migrations. When the maximum observed migration of 50 m and the steepest sand ridges and sand waves are used, the maximum mobile layer depths caused by sand ridge and sand wave migration are 0.9 m and 1.2 m respectively.

(11) Repetitive sidescan surveys have qualitatively established that megaripples, large wave ripples and sand ribbons can be reactivated by annual winter storms or storms of several year return intervals on Sable Island Bank.

Acknowledgements

We would like to thank Hugh Steward and Natalie Stirling of Exxon-Mobil Canada (formerly SOEI) and Roger Ingersoll of Exxon-Mobil for their support and corporation in this joint project. The effort of crews of CCGS Hudson and Creed is appreciated. Support from Dave Heffler was critical for RALPH instrumentation and data reduction. Bob Murphy, Tony Atkinson, Ken Asprey and Bruce Wile provided RALPH preparation, deployment and logistics support. Darrel Beaver, Bob Miller, Randy Currie, Peter Pledge and Bob Covil (TekMap) assisted in multibeam data collection and processing. We have received advice and tips on multibeam data processing from Russ Parrott and John Shaw. Thanks also goes to Don Clattenburg of SEDLAB for sediment grain size analyses. We also would like to thank John Osler and Defence R&D Canada - Atlantic for sharing their sidescan data. Gary Sonnichsen and Steve Solomon critically reviewed this report. This project was jointly funded by Exxon-Mobil Canada (formerly SOEI) and the Panel on Energy Research and Development (PERD) of the Federal Government of Canada through the East Coast Offshore Geotechnics Project 12100E01.

REFERENCES

Amos, C.L. and King, E.L., 1984. Bedforms of the Canadian eastern seaboard: A comparison with global occurrences. Mar. Geol., 57: 167 - 208.

Amos, C.L. and Miller, A., 1990. Quaternary stratigralphy of southwest Sable Island Bank, eastern Canada. GSA Bulletin, 102: 915-934.

Amos, C.L. and Nadeau, O.C., 1988. Surficial sediments of the outer banks, Scotian Shelf, Canada: Canadian Journal of Earth Sciences, 25: 1923 - 1944.

Amos, C.L. and Judge, J.T., 1991. Sediment transport on the eastern Canadian continental shelf. Cont. Shelf Res., 11: 1037-1068.

Amos, C.L., Li, M.Z. and Choung, K-S., 1996. Storm-generated swaley bedding on the outer Scotian Shelf. Geo-Marine Letters, 16: 85-94.

Amos, C. L., M. Z. Li, F. L. Chiocci, G. B. La Monica, S. Cappucci, E. H. King, and F. Corbani, Origin of shore-normal channels from the shoreface of Sable Island, Canada, J. Geophys. Res., 108(C3), doi:10.1029/2001JC001259, 2003.

Courtney, R.C. and Fader, G.B.J., 1994. A new understanding of the ocean floor through multibeam mapping. Science Review 1992 and 1993, Bedford Institute of Oceanography.

Courtney, R.C. and Shaw, J., 2000. Multibeam bathymetry and backscatter imaging of the Canadian continental shelf. Environmental Marine Geoscience 2, Geoscience Canada, 27: 31-42.

Crawford, A., Osler, J., and King, E., Multi-year and hurricane-induced sediment activity on the Scotian Shelf, EOS Trans. AGU, 83 (47), Fall Meet. Suppl., Abstract OS61A-0199, 2002, p. 694.

Dalrymple, R.W. and Hoodendoorn, E.L., 1997. Erosion and deposition on migrating shoreface-attached ridges, Sable Island, Eastern Canada. Geoscience Canada, 24: 25-36.

Dalrymple, R.W., Knight, R.J. and Lambiase, J.J., 1978. Bedforms and their hydraulic stability relationships in a tidal environment, Bay of Fundy, Canada. Nature, 275: 100-104.

Ekman, V.M., 1905. On the influence of the Earth's rotation on ocean-currents. Arkiv for Matematik, Astronomi och Fysik, 2: 1-53.

Folk, R.L. and Ward, W.C., 1957. Brazos River bar: a study in the significance of grain size parameters. Jour. Sed. Petrol., 27: 3-26.

Forsythe, A., 1998. Analysis of geotechnical data for offshore pipeline design: Sable Offshore Energy Project. CE 1404 Civil Engineering Project report, Dalhousie University, 32p.

Hequette, A., Desrosiers, M., Hill, P.R. and Forbes, D.L., 2001. The influence of coastal morphology on shoreface sediment transport under storm-combined flows, Canadian Beaufort Sea. Jour. Coastal Res. 17: 507-516.

Hoogendoorn, E.L., 1989. Sedimentology and dynamics of shoreface-attached ridges, Sable Island Bank, Nova Scotian. Unpublished Ph.D thesis, Queen's University, Kingston, ON, 483 pp.

Hoogendoorn, E.L. and Dalrymple, R.W., 1986. Morphology, lateral migration and internal structures of shoreface-connected ridges, Sable Island Bank, Nova Scotia, Canada. Geology, 14: 400 - 403.

Hudson Cruise 96-029: Sable Island Bank and Laurentian Fan. The participants of the Cruise, 1996. GSCA Internal Cruise Report, 25p.

Ingersoll, R.W. and Ryan, B.A., 1997. Repetitive surveys to assess sand ridge movement offshore Sable Island. Proc. Oceans 97: 1377-1393.

King, L.H., 1970. Surficial geology of the Halifax-Sable Island map area: Canadian Department of Energy, Mines and Resources, Marine Sciences Branch, Paper 1, 16 p.

King, E.L., 2001. A glacial origin for Sable Island: ice and sea-level fluctuations from seismic stratigraphy on Sable Island Bank, Scotian Shelf, offshore Nova Scotia. Geological Survey of Canada, Current Research 2001-D19, 11 p.

King, E.L., 2002. Sable Island Bank shallow geological conditions: Geohazard atlas and catalogue compiled from shallow reflection seismic data. Unpublished Final report to Sable Offshore Energy Incorporated by the Geological Survey of Canada. December 2002.

Lewis, P.J. and Morgan, M.D., 1984. Severe storms off Canada's east coast: A catalogue summary for the period 1957 - 1983. Canadian Climate Centre, Report 84-13 (unpublished manuscript, Atmospheric Environment Service, Downsview).

Li, M.Z. and Amos, C.L., 2001. SEDTRANS96: The Upgraded and Better Calibrated Sediment-Transport Model for Continental Shelves. Computers and Geosciences, 27(6): 619-645.

Li, M.Z., Amos, C.L. and Heffler, D.E., 1997. Boundary layer dynamics and sediment transport under storm and non-storm conditions on the Scotian shelf. Marine Geology, 141: 157-181.

Li, M.Z., Amos, C.L., and Heffler, D.E., 1999. Hydrodynamics and Seabed Stability Observations on Sable Island Bank: A Summary of the Data for 1996/97. Geological Survey of Canada Open File Report 2997.

Li, M.Z., Currie, R., Beaver, D., Girouard, P. and Pledge, P., 1999. Multibeam Surveys of Sable Island Bank and the Gully Area of Scotian Shelf: Report on Creed Cruise 98-100. GSCA Internal Cruise Report, 44 p.

Li, M., Beaver, D., King, E. and Pledge, P., 2001a. Multibeam Surveys of Sable Island Bank, Scotian Shelf: Report on Creed Cruise 2000-100. Geological Survey of Canada Open File 4090, 19 pp.

Li, M. Z., King, E. and cruise participants, 2001b. CSS Hudson Cruise 20000-30a: A Geological and Geophysical Survey on Sable Island Bank and Scotian Shelf. Geological Survey of Canada Open File 4000, 50 pp.

Li, M.Z., King, E., Beaver, D. and Miller, R., 2002. Multibeam Surveys of Sable Island Bank, Scotian Shelf: Report on Creed Cruise 2001-100. Geological Survey of Canada Open File 4301, 36 pp.

Miller, R.O. and cruise participants, 2003. CCGS Hudson Cruise 200221, A Geological and Geophysical Survey on Sable Island Bank. Geological Survey of Canada Open File 1524, 144 pp.

Mobil Oil Canada Ltd., 1983. Venture development project environmental impact statement, vol. IIa, Biophysical assessment. Mobil Oil Canada Ltd., Submitted to Canada Oil and Gas Lands Administration, Ottawa, 415 pp.

Myrow, P.M., 1992. Pot and gutter casts from the Chapel Island Formation, southeast Newfoundland. Journal Sed. Petrology, 62: 992-1007.

Niedoroda, A.W., Swift, D.J.P., and Hopkins, T.S., 1985. The Shoreface, Chapter 8. In: Davis, R.A. Jr. (Ed.), Coastal Sedimentary Environments, 2nd Edition, Springer-Verlag, New York, N.Y., 533-624.

Smyth, C., 2001. A summary of the 2001 Sable Island Bank hydrodynamic and bedform data. (Unpublished) Technical report submitted to GSCA. Contract 23420-01M280.

Swift, D.J.P., Niedoroda, A.W., Vincent, C.E., and Hopkins, T.S., 1985. Barrier island evolution, Middle Atlantic Shelf, U.S.A. Part 1: Shoreface dynamics. Marine Geol., 63: 19 - 42.

Swift, D.J.P. Thorne, J.A. and Oertel, G.F., 1986. Fluid processes and sea-floor response on a modern storm-dominated shelf: Middle Atlantic shelf of North America. Part II: Response of the shelf floor. In: Knight, J.R. and McLean, J.R. (Eds.), Shelf Sands and Sandstones. Canadian Society Petroleum Geologists, Memoir II, 191-211.

Todd, B.J., Fader, G.B., Courtney, R.C. and Pickrill, R.A., 1999. Quaternary geology and surficial sediment processes, Browns Bank, Scotian Shelf, based on multibeam bathymetry. Mar. Geol., 162: 165-214.